

The mathematical theory of resonant transducers in a spherical gravity wave antenna

José Alberto Lobo

Departament de Física Fonamental
Universitat de Barcelona, Spain
e-mail: lobo@hermes.ffn.ub.es

Abstract

Apart from omnidirectional, a solid elastic sphere is a natural multi-mode and multi-frequency device for the detection of Gravitational Waves (GW). Motion sensing in a spherical GW detector thus requires a *multiple* set of transducers attached to it at suitable locations. If these are *resonant* then they exert a significant back action on the larger sphere and, as a consequence, the *joint dynamics* of the entire system must be properly understood before reliable conclusions can be drawn from its readout. In this paper, I present and develop an analytic approach to study such dynamics which generalises currently existing ones and clarifies their actual range of validity. In addition, the new formalism shows that there actually exist resonator layouts alternative to the highly symmetric *TIGA*, potentially having interesting properties. One of these (I will call it *PHC*), which only requires five resonators per quadrupole mode sensed, and has *mode channels*, will be described in detail. Also, the *perturbative* nature of the proposed approach makes it very well adapted to systematically assess the consequences of realistic mistunings in the device parameters by robust analytic methods. In order to check the real value of the mathematical model, its predictions have been confronted with experimental data from the *LSU* prototype detector *TIGA*, and agreement between both is found to consistently reach a satisfactory precision of *four* decimal places.

1 Introduction

The idea of using a solid elastic sphere as a gravitational wave (GW) antenna is almost as old as that of using cylindrical bars: as far back as 1971 Forward published a paper [16] in which he assessed some of the potentialities offered by a spherical solid for that purpose. It was however Weber’s ongoing philosophy and practice of using bars which eventually prevailed and developed up to the present date, with the highly sophisticated and sensitive ultra-cryogenic systems currently in operation —see [8] and [11] for reviews and bibliography. With few exceptions [1, 41], spherical detectors fell into oblivion for years, but interest in them strongly re-emerged in the early 1990’s, and an important number of research articles have been published since which address a wide variety of problems in GW spherical detector science. At the same time, international collaboration has intensified, and prospects for the actual construction of large spherical GW observatories (in the range of ~ 100 tons) are being currently considered in several countries ¹, even in a variant *hollow* shape [12].

A spherical antenna is obviously omnidirectional but, most important, it is also a natural *multi-mode* device, i.e., when suitably monitored, it can generate information on all the GW amplitudes and incidence direction [27], a capability which possesses no other *individual* GW detector, whether resonant or interferometric [14]. Furthermore, a spherical antenna could also reveal the eventual existence of *monopole* gravitational radiation, or set thresholds on it [5].

The theoretical explanation of these facts is to be found in the unique matching between the GW amplitude structure and that of the sphere oscillation eigenmodes [24]: a general *metric* GW generates a *tidal* field of forces in an elastic body which is given in terms of the “electric” components $R_{0i0j}(t)$ of the Riemann tensor at its centre of mass by the following formula [24]:

¹There are collaborations in Brazil, Holland, Italy and Spain.

$$\mathbf{f}_{\text{GW}}(\mathbf{x}, t) = \sum_{\substack{l=0 \text{ and } 2 \\ m=-l, \dots, l}} \mathbf{f}^{(lm)}(\mathbf{x}) g^{(lm)}(t) \quad (1)$$

where $\mathbf{f}^{(lm)}(\mathbf{x})$ are “tidal form factors”, while $g^{(lm)}(t)$ are specific linear combinations of the Riemann tensor components $R_{0i0j}(t)$ which carry all the *dynamical* information on the GW’s monopole ($l=0$) and quadrupole ($l=2$) amplitudes. It is precisely these amplitudes, $g^{(lm)}(t)$, which a GW detector aims to measure.

On the other hand, a free elastic sphere has two families of oscillation eigenmodes, so called *toroidal* and *spheroidal* modes, and modes within either family group into ascending series of l -pole harmonics, each of whose frequencies is $(2l+1)$ -fold degenerate —see [24] for full details. It so happens that *only* monopole and/or quadrupole spheroidal modes can possibly be excited by an incoming *metric* GW [4], and their GW driven amplitudes are directly proportional to the wave amplitudes $g^{(lm)}(t)$ of equation (1). It is this very fact which makes of the spherical detector such a natural one for GW observations [24]. In addition, a spherical antenna has a significantly higher absorption *cross section* than a cylinder of like fundamental frequency, and also presents good sensitivity at the *second* quadrupole harmonic [7].

In order to monitor the GW induced deformations of the sphere *motion sensors* are required. In cylindrical bars, current state of the art technology is based upon *resonant transducers* [9, 17]. A resonant transducer consists in a small (compared to the bar) mechanical device possessing a resonance frequency accurately tuned to that of the cylinder. This *frequency matching* causes back-and-forth *resonant energy transfer* between the two bodies (bar and resonator), which results in turn in *mechanically amplified* oscillations of the smaller resonator. The philosophy of using resonators for motion sensing is directly transplantable to a spherical detector —only a *multiple* set rather than a single resonator is required if its potential capabilities as a multi-mode system are to be exploited to satisfaction.

A most immediate question in a multiple motion sensor system is: *where* should the sensors be? The answer to this basic question naturally depends on design and purpose criteria. Merkowitz and Johnson (M&J) made a very appealing proposal consisting in a set of 6 identical resonators coupling to the *radial* motions of the sphere’s surface, and occupying the positions of the centres of the 6 non-parallel pentagonal faces of a truncated icosahedron [21, 31]. One of the most remarkable properties of such layout is that there exist 5 linear combinations of the resonators’ readouts which are directly proportional to the 5 quadrupole GW amplitudes $g^{(2m)}(t)$ of equation (1). M&J call these combinations *mode channels*, and they therefore play a fundamental role in GW signal deconvolution in a real, *noisy* system [30, 35]. In addition, a reduced scale prototype antenna —called *TIGA*, for *Truncated Icosahedron Gravitational Antenna*— was constructed at Louisiana State University, and its working experimentally put to test [29]. The remarkable success of this experiment in almost every detail [32, 33, 34] stands as a vivid proof of the practical feasibility of a spherical GW detector [3, 36].

Despite its success, the theoretical model proposed by M&J to describe the system dynamics is based upon a simplifying assumption that the resonators *only* couple to the quadrupole vibration modes of the sphere [21, 31]. While this is seen *a posteriori* of experimental measurements to be a very good approximation [29, 33], a deeper *physical* reason which explains *why* this happens is missing so far. The original motivation for the research I present in this article was to develop a more general approach, based on first principles, for the analysis of the resonator problem, very much in the spirit of the methodology and results of reference [24]; this, I thought, would not only provide the necessary tools for a rigorous analysis of the system dynamics, but also contribute to improve our understanding of the physics of the spherical GW detector.

Pursuing this programme, I succeeded in setting up and solving the equations of motion for the coupled system of sphere plus resonators. The most important characteristic of the solution is that it is expressible as a *perturbative series expansion in ascending powers of the small parameter* $\eta^{1/2}$, where η is the ratio between the average resonator’s mass and the sphere’s mass. The dominant (lowest)

order terms in this expansion appear to exactly reproduce Merkowitz and Johnson’s equations [31], whence a quantitative assessment of their degree of accuracy, as well as of the range of validity of their underlying hypotheses obtains; if further precision is required then a well defined procedure for going to next (higher) order terms is unambiguously prescribed by the system equations.

Beyond this, though, the simple and elegant algebra which emerges out of the general scheme has enabled the exploration of different resonator layouts, alternative to the unique *TIGA* of M&J. In particular, I found one [25, 26] requiring 5 rather than 6 resonators per quadrupole mode sensed and possessing the remarkable property that *mode channels* can be constructed from the system readouts, i.e., five linear combinations of the latter which are directly proportional to the five quadrupole GW amplitudes. I called this distribution *PHC* —see below for full details.

The intrinsically perturbative nature of the proposed approach makes it also particularly well adapted to assess the consequences of small defects in the system structure, such as for example symmetry breaking due to suspension attachments, small resonator mistunings and mislocations, etc. This has been successfully applied to account for the reported frequency measurements of the *LSU TIGA* prototype [29], which was diametrically drilled for suspension purposes; in particular, discrepancies between measured and calculated values (generally affecting only the *fourth* decimal place) are precisely of the theoretically predicted order of magnitude.

The method has also been applied to analyse the stability of the spherical detector to several mistuned parameters, with the result that it is not very sensitive to small construction errors. This conforms again to experimental reports [34], but has the advantage that the argument depends on *analytic* mathematical work rather than on computer simulated procedures —see e.g. [34] or [39].

The paper is structured as follows: in section 2, I present the main physical hypotheses of the model, and the general equations of motion. In section 3 a Green function approach to solve those equations is set up, and in section 4 it is used to assess the system response to both monopole and quadrupole GW signals. In section 5 I describe in detail the *PHC* layout, including its frequency spectrum and *mode channels*. Section 6 contains a few brief considerations on the system response to a hammer stroke calibration signal, and finally in section 7 I assess how the different parameter mistunings affect the detector’s behaviour. The paper closes with a summary of conclusions, and three appendices where the heavier mathematical details are made precise for the interested reader.

2 General equations

With minor improvements, I shall use the notation of references [24] and [25], some of which is now briefly recalled. Consider a solid sphere of mass \mathcal{M} , radius R , (uniform) density ϱ , and elastic Lamé coefficients λ and μ , endowed with a set of J resonators of masses M_a and resonance frequencies Ω_a ($a = 1, \dots, J$), respectively. I shall model the latter as *point masses* attached to one end of a linear spring, whose other end is rigidly linked to the sphere at locations \mathbf{x}_a —see Figure 2. The system degrees of freedom are given by the *field* of elastic displacements $\mathbf{u}(\mathbf{x}, t)$ of the sphere plus the *discrete* set of resonator spring deformations $z_a(t)$; equations of motion need to be written down for them, of course, and this is my next concern in this section.

I shall assume that the resonators only move radially, and also that Classical Elasticity theory [23] is sufficiently accurate for the present purposes². In these circumstances we thus have

$$\varrho \frac{\partial^2 \mathbf{u}}{\partial t^2} = \mu \nabla^2 \mathbf{u} + (\lambda + \mu) \nabla (\nabla \cdot \mathbf{u}) + \mathbf{f}(\mathbf{x}, t) \quad (2.a)$$

$$\ddot{z}_a(t) = -\Omega_a^2 [z_a(t) - u_a(t)] + \xi_a^{\text{external}}(t), \quad a = 1, \dots, J \quad (2.b)$$

²We clearly do not expect relativistic motions in extremely small displacements at typical frequencies in the range of 1 kHz.

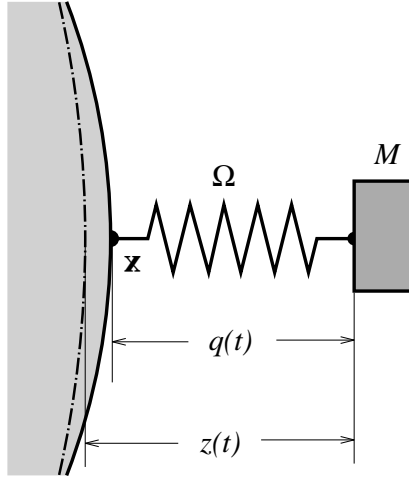


Figure 1: Schematic diagram of the coupling model between a solid sphere and a resonator. The notation is that in the text, but sub-indices have been dropped for clarity. The dashed-dotted arc line on the left indicates the position of the *undeformed* sphere's surface, and the solid arc its *actual* position.

where $\mathbf{n}_a \equiv \mathbf{x}_a/R$ is the outward pointing normal at the the a -th resonator's attachment point, and

$$u_a(t) \equiv \mathbf{n}_a \cdot \mathbf{u}(\mathbf{x}_a, t), \quad a = 1, \dots, J \quad (3)$$

is the *radial* deformation of the sphere's surface at \mathbf{x}_a . A dot ($\dot{}$) is an abbreviation for time derivative. The term in square brackets in (2.b) is thus the spring deformation $-q(t)$ in Figure 2.

$\mathbf{f}(\mathbf{x}, t)$ in the rhs of (2.a) contains the *density* of all *non-internal* forces acting on the sphere, which is expediently split into a component due the resonators' *back action* and an external action *proper*, which can be a GW signal, a calibration signal, etc. Then

$$\mathbf{f}(\mathbf{x}, t) = \mathbf{f}_{\text{resonators}}(\mathbf{x}, t) + \mathbf{f}_{\text{external}}(\mathbf{x}, t) \quad (4)$$

Finally, $\xi_a^{\text{external}}(t)$ in the rhs of (2.b) is the force per unit mass (acceleration) acting on the a -th resonator due to *external* agents.

Given the hypothesis that the resonators are *point masses*, the following holds:

$$\mathbf{f}_{\text{resonators}}(\mathbf{x}, t) = \sum_{a=1}^J M_a \Omega_a^2 [z_a(t) - u_a(t)] \delta^{(3)}(\mathbf{x} - \mathbf{x}_a) \mathbf{n}_a \quad (5)$$

where $\delta^{(3)}$ is the three dimensional Dirac density function.

The *external* forces I shall be considering in this paper will be *gravitational wave* signals, and also a simple calibration signal, a perpendicular *hammer stroke*. GW driving terms, c.f. equation (1), can be written

$$\mathbf{f}_{\text{GW}}(\mathbf{x}, t) = \mathbf{f}^{(00)}(\mathbf{x}) g^{(00)}(t) + \sum_{m=-2}^2 \mathbf{f}^{(2m)}(\mathbf{x}) g^{(2m)}(t) \quad (6)$$

for a general *metric* wave —see [24] for explicit formulas and technical details. While the spatial coefficients $\mathbf{f}^{(lm)}(\mathbf{x})$ are pure *form factors* associated to the *tidal* character of a GW excitation, it is the time dependent factors $g^{(lm)}(t)$ which carry the specific information on the incoming GW. The purpose of a GW detector is to determine the latter coefficients on the basis of suitable measurements.

If a GW sweeps the observatory then the resonators themselves will also be affected, of course. They will be driven, relative to the sphere's centre, by a tidal acceleration which, since they only move radially, is given by

$$\xi_a^{\text{GW}}(t) = c^2 R_{0i0j}(t) x_{a,i} n_{a,j} , \quad a = 1, \dots, J \quad (7)$$

where $R_{0i0j}(t)$ are the “electric” components of the GW Riemann tensor at the centre of the sphere. These can be easily manipulated to give³

$$\xi_a^{\text{GW}}(t) = R \sum_{\substack{l=0 \text{ and } 2 \\ m=-l, \dots, l}} Y_{lm}(\mathbf{n}_a) g^{(lm)}(t) , \quad a = 1, \dots, J \quad (8)$$

where R is the sphere's radius.

I shall also be later considering the response of the system to a particular *calibration* signal, consisting in a hammer stroke with intensity \mathbf{f}_0 , delivered perpendicularly to the sphere's surface at point \mathbf{x}_0 :

$$\mathbf{f}_{\text{stroke}}(\mathbf{x}, t) = \mathbf{f}_0 \delta^{(3)}(\mathbf{x} - \mathbf{x}_0) \delta(t) \quad (9)$$

which is modeled as an impulsive force in both space and time variables. Unlike GW tides, a hammer stroke will be applied on the sphere's surface, so it has no *direct* effect on the resonators. In other words,

$$\xi_a^{\text{stroke}}(t) = 0 , \quad a = 1, \dots, J \quad (10)$$

The fundamental equations thus finally read:

$$\begin{aligned} \varrho \frac{\partial^2 \mathbf{u}}{\partial t^2} &= \mu \nabla^2 \mathbf{u} + (\lambda + \mu) \nabla(\nabla \cdot \mathbf{u}) + \\ &\quad \sum_{b=1}^J M_b \Omega_b^2 [z_b(t) - u_b(t)] \delta^{(3)}(\mathbf{x} - \mathbf{x}_b) \mathbf{n}_b + \mathbf{f}_{\text{external}}(\mathbf{x}, t) \end{aligned} \quad (11.a)$$

$$\ddot{z}_a(t) = -\Omega_a^2 [z_a(t) - u_a(t)] + \xi_a^{\text{external}}(t) , \quad a = 1, \dots, J \quad (11.b)$$

where $\mathbf{f}_{\text{external}}(\mathbf{x}, t)$ will be given by either (6) or (9), as the case may be. Likewise, $\xi_a^{\text{external}}(t)$ will be given by (8) or (10), respectively. The remainder of this paper will be concerned with finding solutions to the system of coupled differential equations (11), and with their meaning and consequences.

3 Green function formalism

In order to solve equations (11) I shall resort to Green function formalism. The essentials of this procedure in the context of the present problem can be found in detail in reference [24]; more specific technicalities are given in appendix A.1.

By means of such formalism equations (11) become the following integro-differential system:

$$u_a(t) = u_a^{\text{external}}(t) + \sum_{b=1}^J \eta_b \int_0^t K_{ab}(t - t') [z_b(t') - u_b(t')] dt' \quad (12.a)$$

$$\ddot{z}_a(t) = \xi_a^{\text{external}}(t) - \Omega_a^2 [z_a(t) - u_a(t)] , \quad a = 1, \dots, J \quad (12.b)$$

³ $Y_{lm}(\mathbf{n})$ are spherical harmonics [15] —see also the multipole expansion of $R_{0i0j}(t)$ in reference [24].

where $u_a^{\text{external}}(t) \equiv \mathbf{n}_a \cdot \mathbf{u}^{\text{external}}(\mathbf{x}_a, t)$, and $\mathbf{u}^{\text{external}}(\mathbf{x}, t)$ is the *bare* (i.e., without attached resonators) sphere's response to the external forces $\mathbf{f}_{\text{external}}(\mathbf{x}, t)$ in the rhs of (11.a). $K_{ab}(t)$ is a *kernel matrix* defined by the following weighted sum of diadic products of wavefunctions⁴:

$$K_{ab}(t) = \Omega_b^2 \sum_N \omega_N^{-1} [\mathbf{n}_b \cdot \mathbf{u}_N^*(\mathbf{x}_b)] [\mathbf{n}_a \cdot \mathbf{u}_N(\mathbf{x}_a)] \sin \omega_N t \quad (13)$$

Finally, the mass ratios of the resonators to the entire sphere are defined by

$$\eta_b \equiv \frac{M_b}{\mathcal{M}}, \quad b = 1, \dots, J \quad (14)$$

and will be *small parameters* in a real device.

Before proceeding further, let us briefly pause for a qualitative inspection of equations (12). Equation (12.a) shows that the sphere's surface deformations $u_a(t)$ are made up of two contributions: one due to the action of *external* agents (GWs or other), contained in $u_a^{\text{external}}(t)$, and another one due to coupling to the resonators. The latter is commanded by the small parameters η_b , and correlates to *all* of the sphere's spheroidal eigenmodes through the kernel matrix $K_{ab}(t)$. This has consequences for GW detectors, for even though GWs may only couple to quadrupole and monopole⁵ spheroidal modes of the *free* sphere [24, 4], attachment of resonators causes, as we see, coupling between these and the *other* modes of the antenna; conversely, the latter back-act on the former, too. As I shall shortly prove, such undesirable effects can be minimised by suitably *tuning* the resonators' frequencies.

3.1 Laplace transform domain equations

A solution to equations (12) will now be attempted. Equation (12.a) is an integral equation belonging in the general class of Volterra equations [40], but the usual iterative solution to it by repeated substitution of $u_b(t)$ into the kernel integral is not viable here due to the *dynamical* contribution of $z_b(t)$, which is in turn governed by the *differential* equation (12.b).

A better suited method to solve this *integro-differential* system is to Laplace-transform it. I denote the Laplace transform of a generic function of time $f(t)$ with a *caret* ($\hat{}$) on its symbol, e.g.,

$$\hat{f}(s) \equiv \int_0^\infty f(t) e^{-st} dt \quad (15)$$

and make the assumption that the system is at rest before an instant of time, $t=0$, say, or

$$\mathbf{u}(\mathbf{x}, 0) = \dot{\mathbf{u}}(\mathbf{x}, 0) = z_a(0) = \dot{z}_a(0) = 0 \quad (16)$$

Equations (12) then adopt the equivalent form

$$\hat{u}_a(s) = \hat{u}_a^{\text{external}}(s) - \sum_{b=1}^J \eta_b \hat{K}_{ab}(s) [\hat{z}_b(s) - \hat{u}_b(s)] \quad (17.a)$$

$$s^2 \hat{z}_a(s) = \hat{\xi}_a^{\text{external}}(s) - \Omega_a^2 [\hat{z}_a(s) - \hat{u}_a(s)], \quad a = 1, \dots, J \quad (17.b)$$

for which use has been made of the *convolution theorem* for Laplace transforms⁶. A further simplification is accomplished if we consider that we shall in practice be only concerned with the *measurable* quantities

⁴The capitalised index N will often be used to imply the multiple index $\{nlm\}$ which characterises the sphere's wavefunctions.

⁵Monopole modes only exist in scalar-tensor theories of gravity, such as e.g. Brans–Dicke [6]; General Relativity of course does not belong in this category.

⁶This theorem states, it is recalled, that the Laplace transform of the convolution product of two functions is the arithmetic product of their respective Laplace transforms.

$$q_a(t) \equiv z_a(t) - u_a(t) , \quad a = 1, \dots, J \quad (18)$$

representing the resonators' actual elastic deformations —cf. Figure 2. It is readily seen that these verify the following:

$$\sum_{b=1}^J \left[\delta_{ab} + \eta_b \frac{s^2}{s^2 + \Omega_a^2} \hat{K}_{ab}(s) \right] \hat{q}_b(s) = -\frac{s^2}{s^2 + \Omega_a^2} \hat{u}_a^{\text{external}}(s) + \frac{\hat{\xi}_a^{\text{external}}(s)}{s^2 + \Omega_a^2} , \quad a = 1, \dots, J \quad (19)$$

Equations (19) constitute a significant simplification of the original problem, as they are a set of just J *algebraic* rather than integral or differential equations. We must solve them for the unknowns $\hat{q}_a(s)$, then perform *inverse Laplace transforms* to revert to $q_a(t)$. I come to this next.

4 System response to a Gravitational Wave

Our concern now is the actual system response when it is acted upon by an incoming GW. It will be calculated by making a number of simplifying assumptions, more precisely:

- i) The detector is perfectly spherical.
- ii) The resonators have identical masses and resonance frequencies.
- iii) The resonators' frequency is accurately matched to one of the sphere's oscillation eigenfrequencies.

It will be shown below (section 7) that a real system can be appropriately treated as one which deviates by definite amounts from this idealised construct. Therefore detailed knowledge of the ideal system behaviour is essential for all purposes: such is the justification for the above simplifications.

The wave-functions $\mathbf{u}_{nlm}(\mathbf{x})$ of an elastic sphere can be found in reference [24] in full detail, and I shall keep the notation of that paper for them. The Laplace transform of the kernel matrix (13) can thus be expressed as —see equation (78) in appendix A.1:

$$\hat{K}_{ab}(s) = \sum_{nl} \frac{\Omega_b^2}{s^2 + \omega_{nl}^2} |A_{nl}(R)|^2 \frac{2l+1}{4\pi} P_l(\mathbf{n}_a \cdot \mathbf{n}_b) \equiv \sum_{nl} \frac{\Omega_b^2}{s^2 + \omega_{nl}^2} \chi_{ab}^{(nl)} \quad (20)$$

where the last term simply *defines* the quantities $\chi_{ab}^{(nl)}$. Note that the sums here extend over the *entire* spectrum of the solid sphere.

The assumption that all the resonators are *identical* simply means that

$$\eta_1 = \dots = \eta_J \equiv \eta , \quad \Omega_1 = \dots = \Omega_J \equiv \Omega \quad (21)$$

The third hypothesis makes reference to the fundamental idea behind using resonators, which is to have them tuned to one of the frequencies of the sphere's spectrum. This is expressed by

$$\Omega = \omega_{n_0 l_0} \quad (22)$$

where $\omega_{n_0 l_0}$ is a specific and *fixed* frequency of the spheroidal spectrum.

In a GW detector it will only make sense to choose $l_0 = 0$ or $l_0 = 2$, as only monopole and quadrupole sphere modes couple to the incoming signal; in practice, n_0 will refer to the first, or perhaps second harmonic [7]. I shall however keep the generic expression (22) for the time being in order to encompass all the possibilities with a unified notation.

Based on the above hypotheses, equation (19) can be rewritten in the form

$$\sum_{b=1}^J \left[\delta_{ab} + \eta \sum_{nl} \frac{\Omega^2 s^2}{(s^2 + \Omega^2)(s^2 + \omega_{nl}^2)} \chi_{ab}^{(nl)} \right] \hat{q}_b(s) = -\frac{s^2}{s^2 + \Omega^2} \hat{u}_a^{\text{GW}}(s) + \frac{\hat{\xi}_a^{\text{GW}}(s)}{s^2 + \Omega^2}, \quad (\Omega = \omega_{n_0 l_0}) \quad (23)$$

where $\hat{\xi}_a^{\text{GW}}(s)$ is the Laplace transform of (8), i.e.,

$$\hat{\xi}_a^{\text{GW}}(s) = R \sum_{\substack{l=0 \text{ and } 2 \\ m=-l, \dots, l}} Y_{lm}(\mathbf{n}_a) \hat{g}^{(lm)}(s), \quad a = 1, \dots, J \quad (24)$$

As mentioned at the end of the previous section, the matrix in the lhs of (23) must now be inverted; this will give us an expression for $\hat{q}_a(s)$, whose *inverse Laplace transform* will take us back to the time domain. A simple glance at the equation suffices however to grasp the unsurmountable difficulties of accomplishing this *analytically*.

Thankfully, though, a *perturbative* approach is applicable when the masses of the resonators are small compared to the mass of the whole sphere, i.e., when the inequality

$$\eta \ll 1 \quad (25)$$

holds. I shall henceforth assume that this is the case, as also is with cylindrical bar resonant transducers. It is shown in appendix A.2 that the perturbative series happens in ascending powers of $\eta^{1/2}$, rather than η itself, and that the lowest order contribution has the form

$$\hat{q}_a(s) = \eta^{-1/2} \sum_{l,m} \hat{\Lambda}_a^{(lm)}(s; \Omega) \hat{g}^{(lm)}(s) + O(0), \quad a = 1, \dots, J \quad (26)$$

where $O(0)$ stands for terms of order η^0 or smaller. Here, $\hat{\Lambda}_a^{(lm)}(s; \Omega)$ is a *transfer function matrix* which relates *linearly* the system response $\hat{q}_a(s)$ to the GW amplitudes $\hat{g}^{(lm)}(s)$, in the usual sense that $q_a(t)$ is given by the *convolution product* of the signal $g^{(lm)}(t)$ with the time domain expression, $\Lambda_a^{(lm)}(t; \Omega)$, of $\hat{\Lambda}_a^{(lm)}(s; \Omega)$. The detector is thus seen to act as a *linear filter* on the GW signal, whose frequency response is characterised by the properties of $\hat{\Lambda}_a^{(lm)}(s; \Omega)$. More specifically, the filter has a number of characteristic frequencies which correspond to the *imaginary parts of the poles* of $\hat{\Lambda}_a^{(lm)}(s; \Omega)$. As also shown in appendix A.2, these frequencies are the symmetric pairs

$$\omega_{a\pm}^2 = \Omega^2 \left(1 \pm \sqrt{\frac{2l+1}{4\pi}} |A_{n_0 l_0}(R)| \zeta_a \eta^{1/2} \right) + O(\eta), \quad a = 1, \dots, J \quad (27)$$

where ζ_a^2 is the a -th eigenvalue of the Legendre matrix

$$P_{l_0}(\mathbf{n}_a \cdot \mathbf{n}_b), \quad a, b = 1, \dots, J \quad (28)$$

associated to the multipole (l_0) selected for tuning —see (22). These frequency pairs correspond to *beats*, typical of resonantly coupled oscillating systems —we shall find them again in section 6 in a particularly illuminating example.

Equation (26) neatly displays the amplification coefficient $\eta^{-1/2}$ of the resonators' motion amplitudes, which corresponds to the familiar resonant energy transfer in coupled systems of linear oscillators [9].

The specific form of the transfer function matrix $\hat{\Lambda}_a^{(lm)}(s; \Omega)$ depends both on the selected mode to tune the resonator frequency Ω and on the resonator distribution geometry. I now come to a discussion of these.

4.1 Monopole gravitational radiation sensing

General Relativity, as is well known, forbids monopole GW radiation. More general *metric* theories, e.g. Brans-Dicke [6], do however predict this kind of radiation. It appears that a spherical antenna is potentially sensitive to monopole waves, so it can serve the purpose of thresholding, or eventually detecting them. It is therefore relevant to consider the system response to scalar waves.

This clearly requires that the resonator set be tuned to a monopole harmonic of the sphere, i.e.,

$$\Omega = \omega_{n0} , \quad (l_0 = 0) \quad (29)$$

where n tags the chosen harmonic —most likely the first ($n=1$) in a thinkable device.

Since $P_0(z) \equiv 1$ (for all z) the eigenvalues of $P_0(\mathbf{n}_a \cdot \mathbf{n}_b)$ are, clearly,

$$\zeta_1^2 = J , \quad \zeta_2^2 = \dots = \zeta_J^2 = 0 \quad (30)$$

for *any resonator distribution*. The tuned mode frequency thus splits into a *single* strongly coupled pair:

$$\omega_{\pm}^2 = \Omega^2 \left(1 \pm \sqrt{\frac{J}{4\pi}} |A_{n0}(R)| \eta^{1/2} \right) + O(\eta) , \quad \Omega = \omega_{n0} \quad (31)$$

The Λ -matrix of equation (26) is seen to be in this case

$$\hat{\Lambda}_a^{(lm)}(s; \omega_{n0}) = (-1)^J \frac{a_{n0}}{\sqrt{J}} \frac{1}{2} \left[(s^2 + \omega_+^2)^{-1} - (s^2 + \omega_-^2)^{-1} \right] \delta_{l0} \delta_{m0} \quad (32)$$

whence the system response is

$$\hat{q}_a(s) = \eta^{-1/2} \frac{(-1)^J}{\sqrt{J}} a_{n0} \frac{1}{2} \left[(s^2 + \omega_+^2)^{-1} - (s^2 + \omega_-^2)^{-1} \right] \hat{g}^{(00)}(s) + O(0) , \quad a = 1, \dots, J \quad (33)$$

regardless of resonator positions. The overlap coefficient a_{n0} is given in [24]⁷, and can be calculated by means of numerical computer programmes. By way of example, $a_{10}/R = 0.214$, and $a_{20}/R = -0.038$ for the first two harmonics.

A few interesting facts are displayed by equation (33). First, as already stressed, it is seen that if the resonators are tuned to a monopole *detector* frequency then only monopole *wave amplitudes* couple strongly to the system, even if quadrupole radiation amplitudes are significantly high at the observation frequencies ω_{\pm} . Also, the amplitudes $\hat{q}_a(s)$ are equal for all a , as corresponds to the spherical symmetry of monopole sphere's oscillations, and are proportional to $J^{-1/2}$, a factor we should indeed expect as an indication that GW *energy* is evenly distributed amongst all the resonators. A *single* transducer suffices to experimentally determine the only monopole GW amplitude $\hat{g}^{(00)}(s)$, of course, but (33) provides the system response if more than one sensor is mounted on the antenna for whatever reasons.

4.2 Quadrupole gravitational radiation sensing

I now consider the more interesting case of quadrupole motion sensing. The choice is now, clearly,

$$\Omega = \omega_{n2} , \quad (l_0 = 2) \quad (34)$$

where n labels the chosen harmonic —most likely the first ($n=1$) or the second ($n=2$) in a practical system. The evaluation of the Λ -matrix is now considerably more involved [38], yet a remarkably elegant form is found for it:

⁷Please note that there is a small notation change: what I call a_{n0} here is a_n in [24].

$$\hat{\Lambda}_a^{(lm)}(s; \omega_{n2}) = (-1)^N \sqrt{\frac{4\pi}{5}} a_{n2} \sum_{b=1}^J \left\{ \sum_{\zeta_c \neq 0} \frac{1}{2} \left[(s^2 + \omega_{c+}^2)^{-1} - (s^2 + \omega_{c-}^2)^{-1} \right] \frac{v_a^{(c)} v_b^{(c)*}}{\zeta_c} \right\} Y_{2m}(\mathbf{n}_b) \delta_{l2} \quad (35)$$

where $v_a^{(c)}$ is the c -th normalised eigenvector of $P_2(\mathbf{n}_a \cdot \mathbf{n}_b)$, associated to the *non-null* eigenvalue ζ_c^2 . Let me stress that equation (35) explicitly shows that at most 5 pairs of modes, of frequencies $\omega_{c\pm}$, couple strongly to quadrupole GW amplitudes, *no matter how many resonators in excess of 5 are mounted on the sphere*. The tidal overlap coefficients a_{n2} can also be calculated (cf. [24]⁸, and give for the first two harmonics

$$\frac{a_{12}}{R} = 0.328, \quad \frac{a_{22}}{R} = 0.106 \quad (36)$$

The system response is thus

$$\begin{aligned} \hat{q}_a(s) &= \eta^{-1/2} (-1)^J \sqrt{\frac{4\pi}{5}} a_{n2} \sum_{b=1}^J \left\{ \sum_{\zeta_c \neq 0} \frac{1}{2} \left[(s^2 + \omega_{c+}^2)^{-1} - (s^2 + \omega_{c-}^2)^{-1} \right] \frac{v_a^{(c)} v_b^{(c)*}}{\zeta_c} \right\} \times \\ &\quad \times \sum_{m=-2}^2 Y_{2m}(\mathbf{n}_b) \hat{g}^{(2m)}(s) + O(0), \quad a = 1 \dots, J \end{aligned} \quad (37)$$

Equation (37) is *completely general*, i.e., it is valid for any resonator configuration over the sphere's surface, and for any number of resonators. It describes precisely how all 5 GW amplitudes $\hat{g}^{(2m)}(s)$ interact with all 5 strongly coupled system modes; like before, *only quadrupole wave amplitudes* are seen in the detector (to leading order) when $\Omega = \omega_{n2}$, even if the incoming wave carries significant monopole energy at the frequencies $\omega_{c\pm}$.

The degree of generality and algebraic simplicity of (37) is new in the literature. As we shall now see, it makes possible a systematic search for different resonator distributions and their properties.

5 The *PHC* configuration

Merkowitz and Johnson's *TIGA* [21] is highly symmetric, and is the minimal set with maximum degeneracy, i.e., all the non-null eigenvalues ζ_a are equal. To accomplish this, however, 6 rather than 5 resonators are required on the sphere's surface. Since there are just 5 quadrupole GW amplitudes one may wonder whether there are alternative layouts with *only* 5 resonators. Equation (37) is completely general, so it can be searched for an answer to this question. In reference [25] a specific proposal was made, which I now describe in detail.

In pursuing a search for 5 resonator sets I found that distributions having a sphere diameter as an axis of *pentagonal symmetry*⁹ exhibit a rather appealing structure. More specifically, let the resonators be located at the spherical positions

$$\theta_a = \alpha \quad (\text{all } a), \quad \varphi_a = (a-1) \frac{2\pi}{5}, \quad a = 1, \dots, 5 \quad (38)$$

The eigenvalues and eigenvectors of $P_2(\mathbf{n}_a \cdot \mathbf{n}_b)$ are easily calculated:

⁸Please note that there is a small notation change: what I call a_{n2} here is b_n in [24].

⁹By this I mean resonators are placed along a *parallel* of the sphere every 72° .

$$\zeta_0^2 = \frac{5}{4} (3 \cos^2 \alpha - 1)^2, \quad \zeta_1^2 = \zeta_{-1}^2 = \frac{15}{2} \sin^2 \alpha \cos^2 \alpha, \quad \zeta_2^2 = \zeta_{-2}^2 = \frac{15}{8} \sin^4 \alpha \quad (39.a)$$

$$v_a^{(m)} = \sqrt{\frac{4\pi}{5}} \zeta_m^{-1} Y_{2m}(\mathbf{n}_a), \quad m = -2, \dots, 2, \quad a = 1, \dots, 5 \quad (39.b)$$

so the Λ -matrix is also considerably simple in structure in this case:

$$\hat{\Lambda}_a^{(lm)}(s; \omega_{n2}) = -\sqrt{\frac{4\pi}{5}} a_{n2} \zeta_m^{-1} \frac{1}{2} \left[\left(s^2 + \omega_{m+}^2 \right)^{-1} - \left(s^2 + \omega_{m-}^2 \right)^{-1} \right] Y_{2m}(\mathbf{n}_a) \delta_{l2}, \quad PHC \quad (40)$$

where the notation

$$\omega_{m\pm}^2 = \Omega^2 \left(1 \pm \sqrt{\frac{5}{4\pi}} |A_{n2}(R)| \zeta_m \eta^{1/2} \right) + O(\eta), \quad m = -2, \dots, 2 \quad (41)$$

has been used. As seen in these formulas, the *five* expected pairs of frequencies actually reduce to *three*, so pentagonal distributions keep a certain degree of degeneracy, too. The most important distinguishing characteristic of the general *pentagonal* layout is best displayed by the explicit system response:

$$\begin{aligned} \hat{q}_a(s) &= -\eta^{-1/2} \sqrt{\frac{4\pi}{5}} a_{n2} \\ &\times \left\{ \frac{1}{2\zeta_0} \left[\left(s^2 + \omega_{0+}^2 \right)^{-1} - \left(s^2 + \omega_{0-}^2 \right)^{-1} \right] Y_{20}(\mathbf{n}_a) \hat{g}^{(20)}(s) \right. \\ &+ \frac{1}{2\zeta_1} \left[\left(s^2 + \omega_{1+}^2 \right)^{-1} - \left(s^2 + \omega_{1-}^2 \right)^{-1} \right] \left[Y_{21}(\mathbf{n}_a) \hat{g}^{(11)}(s) + Y_{2-1}(\mathbf{n}_a) \hat{g}^{(1-1)}(s) \right] \\ &\left. + \frac{1}{2\zeta_2} \left[\left(s^2 + \omega_{2+}^2 \right)^{-1} - \left(s^2 + \omega_{2-}^2 \right)^{-1} \right] \left[Y_{22}(\mathbf{n}_a) \hat{g}^{(22)}(s) + Y_{2-2}(\mathbf{n}_a) \hat{g}^{(2-2)}(s) \right] \right\} \quad (42) \end{aligned}$$

This equation indicates that *different wave amplitudes selectively couple to different detector frequencies*. This should be considered a very remarkable fact, for it thence follows that simple inspection of the system readout *spectrum*¹⁰ immediately reveals whether a given wave amplitude $\hat{g}^{2m}(s)$ is present in the incoming signal or not.

Pentagonal configurations also admit *mode channels*, which are easily constructed from (42) thanks to the orthonormality property of the eigenvectors (39.b):

$$\hat{y}^{(m)}(s) \equiv \sum_{a=1}^5 v_a^{(m)*} \hat{q}_a(s) = \eta^{-1/2} a_{n2} \frac{1}{2} \left[\left(s^2 + \omega_{m+}^2 \right)^{-1} - \left(s^2 + \omega_{m-}^2 \right)^{-1} \right] \hat{g}^{(2m)}(s) + O(0) \quad (43)$$

These are almost identical to the *TIGA* mode channels [31], the only difference being that each mode channel comes now at a *single specific* frequency pair $\omega_{m\pm}$.

Mode channels are fundamental in signal deconvolution algorithms in noisy systems [30, 35]. Pentagonal resonator configurations should thus be considered non-trivial candidates for a real GW detector.

Based on these facts one may next ask which is a suitable transducer distribution with an axis of pentagonal symmetry. Figure 2 shows a plot of the eigenvalues (39.a) as functions of α , the angular distance of the resonator set from the symmetry axis. Several criteria may be adopted to select a specific choice in view of this graph. An interesting one can be arrived at by the following argument. If for ease of mounting, stability, etc., it is desirable to have the detector milled into a close-to-spherical

¹⁰In a noiseless system, of course.

polyhedric shape¹¹ then polyhedra with axes of pentagonal symmetry must be searched. The number of quasi regular *convex* polyhedra is of course finite —there actually are only 18 of them [20, 18]—, and I found a particularly appealing one in the so called *pentagonal hexacontahedron* (*PHC*), displayed in Figure 3, left —see also [25]. This is a 60 face polyhedron, whose faces are the identical *irregular pentagons* of Figure 3, right. The *PHC* admits an *inscribed sphere* which is tangent to each face at the central point marked in the Figure. It is clearly to this point that a resonator should be attached so as to simulate an as perfect as possible spherical distribution.

The *PHC* is considerably spherical: the ratio of its volume to that of the inscribed sphere is 1.057, which quite favourably compares to the value of 1.153 for the ratio of the circumscribed sphere to the TI volume. If the frequency pairs $\omega_{m\pm}$ are now requested to be as *evenly spaced* as possible, compatible with the *PHC* face orientations, then the choice $\alpha = 67.617^\circ$ is unambiguously singled out. Hence

$$\omega_{0\pm} = \omega_{12} \left(1 \pm 0.5756 \eta^{1/2}\right), \quad \omega_{1\pm} = \omega_{12} \left(1 \pm 0.8787 \eta^{1/2}\right), \quad \omega_{2\pm} = \omega_{12} \left(1 \pm 1.0668 \eta^{1/2}\right) \quad (44)$$

for instance for $\Omega = \omega_{12}$, the first quadrupole harmonic. Figure 4 shows this frequency spectrum together with the multiply degenerate *TIGA* for comparison.

The criterion leading to the *PHC* proposal is of course not unique, and alternatives can be considered. For example, if the 5 faces of a regular icosahedron are selected for sensor mounting ($\alpha = 63.45^\circ$) then a four-fold degenerate pair plus a single non-degenerate pair is obtained; if the resonator parallel is 50° or 22.6° away from the “north pole” then the three frequencies ω_{0+} , ω_{1+} , and ω_{2+} are equally spaced; etc. The number of choices is virtually infinite if the sphere is not milled into a polyhedric shape [39, 28].

Let me finally recall that the complete *PHC* proposal [25] was made with the idea of building an as complete as possible spherical GW antenna, which amounts to making it sensitive at the first *two* quadrupole frequencies *and* at the first monopole one. This would take advantage of the good sphere cross section at the second quadrupole harmonic [7], and would enable measuring (or thresholding) eventual monopole GW radiation. Now, the system *pattern matrix* $\hat{\Lambda}_a^{(lm)}(s; \Omega)$ has *identical structure* for all the harmonics of a given l series —see (32) and (35)—, and so too identical criteria for resonator layout design apply to either set of transducers, respectively tuned to ω_{12} and ω_{22} . The *PHC* proposal is best described graphically in Figure 3, left: a *second* set of resonators, tuned to the second quadrupole harmonic ω_{22} can be placed in an equivalent position in the “southern hemisphere”, and an eleventh resonator tuned to the first monopole frequency ω_{10} is added at an arbitrary position. It is not difficult to see, by the general methods outlined earlier on in this paper, that cross interaction between these three sets of resonators is only *second order* in $\eta^{1/2}$, therefore weak.

A spherical GW detector with such a set of altogether 11 transducers would be a very complete multi-mode multi-frequency device with an unprecedented capacity as an individual antenna. Amongst other, it would practically enable monitoring of coalescing binary *chirp* signals by means of a rather robust double passage method [10], a prospect which was considered so far possible only with broadband long baseline laser interferometers [13, 22], and is almost unthinkable with currently operating cylindrical bars.

6 A calibration signal: hammer stroke

This section is a brief digression from the main streamline of the paper. I propose to assess now the system response to a particular, but useful, calibration signal: a perpendicular *hammer stroke*.

Let us first go back to equation (19) and replace $\hat{u}_a^{\text{external}}(s)$ in its rhs with that corresponding to a hammer stroke, which is easily calculated —cf. appendix A.1:

¹¹This is the philosophy suggested and experimentally implemented by Merkowitz and Johnson at *LSU*.

$$\hat{u}_a^{\text{stroke}}(s) = - \sum_{nl} \frac{f_0}{s^2 + \omega_{nl}^2} |A_{nl}(R)|^2 P_l(\mathbf{n}_a \cdot \mathbf{n}_0), \quad a = 1, \dots, J \quad (45)$$

where \mathbf{n}_0 are the spherical coordinates of the hit point on the sphere, and $f_0 \equiv \mathbf{n}_0 \cdot \mathbf{f}_0 / \mathcal{M}$. Clearly, the hammer stroke excites *all* of the sphere's vibration eigenmodes, as it has a completely flat spectrum.

The coupled system resonances are again those calculated in appendix A.2. The same procedures described in section 4 for a GW excitation can now be pursued to obtain

$$\begin{aligned} \hat{q}_a(s) &= \eta^{-1/2} (-1)^{J-1} \sqrt{\frac{2l+1}{4\pi}} f_0 |A_{nl}(R)| \times \\ &\times \sum_{b=1}^J \left\{ \sum_{\zeta_c \neq 0} \frac{1}{2} \left[(s^2 + \omega_{c+}^2)^{-1} - (s^2 + \omega_{c-}^2)^{-1} \right] \frac{v_a^{(c)} v_b^{(c)*}}{\zeta_c} \right\} P_l(\mathbf{n}_b \cdot \mathbf{n}_0) + O(0) \end{aligned} \quad (46)$$

where $a = 1, \dots, J$, when the system is tuned to the nl -th spheroidal harmonic, i.e., $\Omega = \omega_{nl}$. It is immediately seen from here that the system response to this signal when the resonators are tuned to a *monopole* frequency is given by

$$\hat{q}_a(s) = \eta^{-1/2} (-1)^{J-1} \frac{f_0}{\sqrt{4\pi J}} |A_{n0}(R)| \frac{1}{2} \left[(s^2 + \omega_+^2)^{-1} - (s^2 + \omega_-^2)^{-1} \right], \quad \Omega = \omega_{n0} \quad (47)$$

an expression which holds for all a , and is independent of either the resonator layout or the hit point, which in particular prevents any determination of the latter, as obviously expected. The frequencies ω_{\pm} are those of (31), and we find here again a global factor $J^{-1/2}$, as also expected.

Consider next the situation when quadrupole tuning is implemented, $\Omega = \omega_{n2}$. Only the *PHC* and *TIGA* configurations will be addressed, as more general cases are not quite as interesting at this point.

6.1 PHC and TIGA response to a hammer stroke

Expanding equation (46) by substitution of the eigenvalues ζ_m and eigenvectors $v_a^{(m)}$ of the *PHC*, one readily finds that the system response is given by

$$\hat{q}_a(s) = \eta^{-1/2} f_0 \sqrt{\frac{4\pi}{5}} |A_{n2}(R)| \sum_{m=-2}^2 \frac{1}{2} \left[(s^2 + \omega_{m+}^2)^{-1} - (s^2 + \omega_{m-}^2)^{-1} \right] \zeta_m^{-1} Y_{2m}(\mathbf{n}_a) Y_{2m}^*(\mathbf{n}_0) \quad (48)$$

with $a = 1, \dots, 5$, and the mode channels by

$$\hat{y}^{(m)}(s) = \eta^{-1/2} f_0 |A_{n2}(R)| \frac{1}{2} \left[(s^2 + \omega_{m+}^2)^{-1} - (s^2 + \omega_{m-}^2)^{-1} \right] Y_{2m}^*(\mathbf{n}_0), \quad m = -2, \dots, 2 \quad (49)$$

These equations indicate that the system response $q_a(t)$ is a *superposition of three different beats*¹², while the mode channels are *single* beats each, but with *differing modulation frequencies*. This is represented graphically in Figure 5, where we see the result of a numerical simulation of the *PHC* response to a hammer stroke, delivered to the solid at a given location. The readouts $q_a(t)$ are somewhat complex time series, whose frequency spectrum shows *three pairs of peaks* —in fact, the *lines* in the

¹²A *beat* is a modulated oscillation of the form $\sin \frac{1}{2}(\omega_+ - \omega_-)t \cos \Omega t$, where ω_+ and ω_- are nearby frequencies, and $\omega_+ + \omega_- = 2\Omega$. The Laplace transform of such function of time is precisely $(\Omega/2) \left[(s^2 + \omega_+^2)^{-1} - (s^2 + \omega_-^2)^{-1} \right]$, up to higher order terms in the difference $\omega_+ - \omega_-$, which in this case is proportional to $\eta^{1/2}$.

ideal spectrum of Figure 4. The mode channels on the other hand are *pure beats*, whose spectra consist of the *individually separate* pairs of the just mentioned peaks.

The response of the *TIGA* layout to a hammer stroke has been described in detail by Merkowitz and Johnson —see e.g. reference [33]. The present formalism does of course lead to the results obtained by them; in the notation of this paper, we have

$$\hat{q}_a(s) = -\eta^{-1/2} \frac{5}{\sqrt{24\pi}} f_0 |A_{n2}(R)| \frac{1}{2} \left[(s^2 + \omega_+^2)^{-1} - (s^2 + \omega_-^2)^{-1} \right] P_2(\mathbf{n}_a \cdot \mathbf{n}_0) \quad (50.a)$$

$$\hat{y}^{(m)}(s) = -\eta^{-1/2} f_0 |A_{n2}(R)| \frac{1}{2} \left[(s^2 + \omega_+^2)^{-1} - (s^2 + \omega_-^2)^{-1} \right] Y_{2m}^*(\mathbf{n}_0), \quad m = -2, \dots, 2 \quad (50.b)$$

for the system response and the mode channels, respectively, where

$$\omega_{\pm}^2 = \omega_{n2}^2 \left(1 \pm \sqrt{\frac{3}{2\pi}} |A_{n2}(R)| \eta^{1/2} \right) + O(\eta), \quad a = 1, \dots, 6 \quad (51)$$

are the five-fold degenerate frequency pairs corresponding to the *TIGA* distribution. Comparison of the mode channels shows that they are identical for *PHC* and *TIGA*, except that the former come at different frequencies depending on the index m . One might perhaps say that the *PHC* gives rise to a sort of “Zeeman splitting” of the *TIGA* degenerate frequencies, which can be attributed to an *axial symmetry breaking* of that resonator distribution: the *PHC* mode channels partly split up the otherwise degenerate multiplet into its components.

7 Symmetry defects

So far we have made the assumption that the sphere is perfectly symmetric, that the resonators are identical, that their locations on the sphere’s surface are ideally accurate, etc. This is of course unrealistic. So I propose to address now how departures from such ideal conditions affect the system behaviour. As we shall see, the system is rather *robust*, in a sense to be made precise shortly, against a number of small defects.

In order to *quantitatively* assess ideality failures I shall adopt a philosophy which is naturally suggested by the results already obtained in an ideal system. It is as follows.

As seen in previous sections, the solution to the general equations (19) must be given as a *perturbative* series expansion in ascending powers of the small quantity $\eta^{1/2}$. This is clearly a fact *not* related to the system’s symmetries, so it will survive symmetry breakings. It is therefore appropriate to *parametrise* deviations from ideality in terms of suitable powers of $\eta^{1/2}$, in order to address them *consistently with the order of accuracy of the series solution to the equations of motion*. An example will better illustrate the situation.

In a *perfectly ideal* spherical detector the system frequencies are given by equations (27). Now, if a small departure from e.g. spherical symmetry is present in the system then we expect that a correspondingly small correction to those equations will be required. Which specific correction to the formula will actually happen can be *qualitatively* assessed by a *consistency* argument: if symmetry defects are of order $\eta^{1/2}$ then equations (27) will be significantly altered in their $\eta^{1/2}$ terms; if on the other hand such defects are of order η or smaller then any modifications to equations (27) will be swallowed into the $O(0)$ terms, and the more important $\eta^{1/2}$ terms will remain unaffected by the symmetry failure. One can say in this case that the system is *robust* against that symmetry breaking.

More generally, this argument can be extended to see that the only system defects standing a chance to have any influences on lowest order ideal system behaviour are defects of order $\eta^{1/2}$ relative to an ideal configuration. Defects of such order are however *not necessarily guaranteed* to be significant, and a specific analysis is required for each concrete parameter in order to see whether or not the system

response is *robust* against the considered parameter deviations. Let us now go into the quantitative detail.

Let P be one of the system parameters, e.g. a sphere frequency, or a resonator mass or location, etc. Let P_{ideal} be the *numerical value* this parameter has in an ideal detector, and let P_{real} be its value in the real case. These two will be assumed to differ by terms of order $\eta^{1/2}$, i.e.,

$$P_{\text{real}} = P_{\text{ideal}} (1 + p \eta^{1/2}) \quad (52)$$

For a given system, p is readily determined adopting (52) as the *definition* of P_{real} , once a suitable *hypothesis* has been made as to which is the value of P_{ideal} . In order for the following procedure to make sensible sense it is clearly required that p be of order 1 or, at least, appreciably larger than $\eta^{1/2}$. Should p thus calculated from (52) happen to be too small, i.e., of order $\eta^{1/2}$ itself or smaller, then the system will be considered *robust* as regards the affected parameter.

7.1 The suspended sphere

An earth based observatory obviously requires a *suspension mechanism* for the large sphere. If a *nodal point* suspension is e.g. selected then a diametral *bore* has to be drilled across the sphere [29]. The most immediate consequence of this is that spherical symmetry is broken, what in turn results in *degeneracy lifting* of the free spectral frequencies ω_{nl} , which now *split* up into multiplets ω_{nlm} ($m = -l, \dots, l$). The resonators' frequency Ω *cannot* therefore be matched to *the* frequency $\omega_{n_0 l_0}$, but at most to *one* of the $\omega_{n_0 l_0 m}$'s. In this subsection I keep the hypothesis —to be relaxed later, see below— that all the resonators are identical, and assume that Ω falls *within* the span of the multiplet of the $\omega_{n_0 l_0 m}$'s. Then

$$\omega_{n_0 l_0 m}^2 = \Omega^2 (1 + p_m \eta^{1/2}), \quad m = -l_0, \dots, l_0 \quad (53)$$

The coupled frequencies, i.e., the roots of equation (86), will now be searched. The kernel matrix $\hat{K}_{ab}(s)$ is however no longer given by (20), due the removed degeneracy of ω_{nl} , and we must stick to its general expression (75), or

$$\hat{K}_{ab}(s) = \sum_{nlm} \frac{\Omega_b^2}{s^2 + \omega_{nlm}^2} |A_{nl}(R)|^2 \frac{2l+1}{4\pi} Y_{lm}^*(\mathbf{n}_a) Y_{lm}(\mathbf{n}_b) \equiv \sum_{nlm} \frac{\Omega_b^2}{s^2 + \omega_{nlm}^2} \chi_{ab}^{(nlm)} \quad (54)$$

Following the steps of appendix A.1 we now seek the roots of the equation

$$\det \left[\delta_{ab} + \eta \sum_{m=-l_0}^{l_0} \frac{\Omega^2 s^2}{(s^2 + \Omega^2)(s^2 + \omega_{n_0 l_0 m}^2)} \chi_{ab}^{(n_0 l_0 m)} + \eta \sum_{nl \neq n_0 l_0, m} \frac{\Omega^2 s^2}{(s^2 + \Omega^2)(s^2 + \omega_{nlm}^2)} \chi_{ab}^{(nlm)} \right] = 0 \quad (55)$$

Since Ω relates to $\omega_{n_0 l_0 m}$ through equation (53) we see that the roots of (55) fall again into either of the two categories (89) (see Appendix A.2), i.e., roots close to $\pm i\Omega$ and roots close to $\pm i\omega_{nlm}$ ($nl \neq n_0 l_0$). I shall exclusively concentrate on the former now. Direct substitution of the series (89.a) into (55) yields the following equation for the coefficient $\chi_{\frac{1}{2}}$:

$$\det \left[\delta_{ab} - \frac{1}{\chi_{\frac{1}{2}}} \sum_{m=-l_0}^{l_0} \frac{\chi_{ab}^{(n_0 l_0 m)}}{\chi_{\frac{1}{2}} - p_m} \right] = 0 \quad (56)$$

This is a variation of (90), to which it reduces when $p_m = 0$, i.e., when there is full degeneracy.

The solutions to (56) no longer come in symmetric pairs, like (27). Rather, there are $2l_0+1+J$ of them, with a *maximum* number of $2(2l_0+1)$ non-identically zero roots if $J \geq 2l_0+1$ ¹³. For example, if

¹³This is a *mathematical fact*, whose proof is relatively cumbersome, and will be omitted here; let me just mention that it has its origin in the linear dependence of more than $2l_0+1$ spherical harmonics of order l_0 .

we choose to select the resonators' frequency close to a quadrupole multiplet ($l_0 = 2$) then (56) has at most $5+J$ non-null roots, *with a maximum ten* no matter how many resonators in excess of 5 we attach to the sphere. Modes associated to null roots of (56) can be seen to be *weakly coupled*, just like in a free sphere, i.e., their amplitudes are smaller than those of the strongly coupled ones by factors of order $\eta^{1/2}$.

In order to assess the reliability of this method I have applied it to see what are its predictions for a *real system*. To this end, data taken with the *TIGA* prototype at *LSU*¹⁴ were used to confront with. The *TIGA* was drilled and suspended from the centre, so its first quadrupole frequency split up into a multiplet of five frequencies. Their reportedly measured values are

$$\omega_{120} = 3249 \text{ Hz} , \quad \omega_{121} = 3238 \text{ Hz} , \quad \omega_{12-1} = 3236 \text{ Hz} , \quad \omega_{122} = 3224 \text{ Hz} , \quad \omega_{12-2} = 3223 \text{ Hz} , \quad (57)$$

All 6 resonators were equal, and had the following characteristic frequency and mass, respectively:

$$\Omega = 3241 \text{ Hz} , \quad \eta = \frac{1}{1762.45} \quad (58)$$

Substituting these values into (53) it is seen that

$$p_0 = 0.2075 , \quad p_1 = -0.0777 , \quad p_{-1} = -0.1036 , \quad p_2 = -0.4393 , \quad p_{-2} = -0.4650 \quad (59)$$

Equation (56) can now be readily solved, once the resonator positions are fed into the matrices $\chi_{ab}^{(12m)}$. Such positions correspond to the pentagonal faces of a truncated icosahedron. Merkwitz [29] gives a complete account of all the measured system frequencies as resonators are progressively attached to the selected faces, beginning with one and ending with six. Figure 6 graphically displays the experimentally reported frequencies along with those calculated theoretically by solving equation (56). In Table 1 I give the numerical values. As can be seen, coincidence between theoretical predictions and experimental data is remarkable: the worst error is 0.2%, while for the most part it is below 0.1%. This is a few parts in 10^4 , which is precisely the magnitude of η , as specified in equation (58).

Therefore *discrepancies between theoretical predictions and experimental data are exactly as expected*, i.e., of order η . In addition, it is also reported in reference [33] that the 11-th, weakly coupled mode of the *TIGA* (enclosed in square brackets in Table 1) has a practically zero amplitude, again in excellent agreement with the general theoretical predictions about modes beyond the tenth —see paragraph after equation (56).

This is a remarkable result which encouraged a better fit by estimates of *next order* corrections, i.e., χ_1 of (89.a). As it turned out, however, matching between theory and experiment does not consistently improve in the next step. This is not really that surprising, though, as M&J explicitly state [33] that control of the general experimental conditions in which data were obtained had a certain degree of tolerance, and they actually show satisfaction that $\sim 1\%$ coincidence between theory and measurement is comfortably accomplished. But 1% is *two orders of magnitude larger than η* —cf. equation (58)—, so failure to refine our frequency estimates to order η is again fully consistent with the accuracy of available real data.

A word on a technical issue is in order. Merkwitz and Johnson's equations for the *TIGA* [21, 31] are identical to the equations in this paper to lowest order in η . Remarkably, though, their reported theoretical estimates of the system frequencies are not quite as accurate as those in Table 1 [33]. The reason is probably this: in M&J's model these frequencies appear within an algebraic system of $5+J$ linear equations with as many unknowns which has to be solved; here instead the algebraic system has only J equations and unknowns, actually equations (19). This is a very appreciable difference for the range of values of J under consideration. While the roots for the frequencies *mathematically* coincide in both approaches, in actual practice they are *estimated*, generally by means of computer programmes.

¹⁴These data are contained in reference [29]; I want to thank Stephen Merkwitz for kindly handing them to me.

Table 1: Numerical values of measured and theoretically predicted frequencies (in Hz) for the *TIGA* prototype with varying number of resonators. Relative errors are also shown as parts in 10^4 . The *calculated* values of the tuning and free multiplet frequencies are taken *by definition* equal to the measured ones, and quoted in brackets. In square brackets the frequency of the *weakly coupled* sixth mode in the full, 6 resonator *TIGA* layout. These data are plotted in Figure 6.

| Descr. | Meas. | Calc. | Difference (parts in 10^4) | Descr. | Meas. | Calc. | Difference (parts in 10^4) |
|-----------|-------|--------|----------------------------------|----------|--------|--------|----------------------------------|
| Tuning | 3241 | (3241) | (0) | 4 reson. | 3159 | 3155 | -12 |
| No reson. | 3223 | (3223) | (0) | | 3160 | 3156 | -11 |
| | 3224 | (3224) | (0) | | 3168 | 3165 | -12 |
| | 3236 | (3236) | (0) | | 3199 | 3198 | -5 |
| | 3238 | (3238) | (0) | | 3236 | 3236 | 0 |
| | 3249 | (3249) | (0) | | 3285 | 3286 | 3 |
| 1 reson. | 3167 | 3164 | -8 | | 3310 | 3310 | 0 |
| | 3223 | 3223 | 0 | | 3311 | 3311 | 0 |
| | 3236 | 3235 | -2 | | 3319 | 3319 | 0 |
| | 3238 | 3237 | -2 | 5 reson. | 3152 | 3154 | 8 |
| | 3245 | 3245 | 0 | | 3160 | 3156 | -14 |
| | 3305 | 3307 | 6 | | 3163 | 3162 | -3 |
| 2 reson. | 3160 | 3156 | -13 | | 3169 | 3167 | -8 |
| | 3177 | 3175 | -7 | | 3209 | 3208 | -2 |
| | 3233 | 3233 | 0 | | 3268 | 3271 | 10 |
| | 3236 | 3236 | 0 | | 3304 | 3310 | 17 |
| | 3240 | 3240 | 0 | | 3310 | 3311 | 3 |
| | 3302 | 3303 | 3 | | 3313 | 3316 | 10 |
| | 3311 | 3311 | 0 | | 3319 | 3321 | 6 |
| 3 reson. | 3160 | 3155 | -15 | 6 reson. | 3151 | 3154 | 11 |
| | 3160 | 3156 | -13 | | 3156 | 3155 | -3 |
| | 3191 | 3190 | -2 | | 3162 | 3162 | 0 |
| | 3236 | 3235 | -2 | | 3167 | 3162 | -14 |
| | 3236 | 3236 | 0 | | 3170 | 3168 | -7 |
| | 3297 | 3299 | 8 | | [3239] | [3241] | [6] |
| | 3310 | 3311 | 2 | | 3302 | 3309 | 23 |
| | 3311 | 3311 | 0 | | 3308 | 3310 | 6 |
| | | | | | 3312 | 3316 | 12 |
| | | | | | 3316 | 3317 | 2 |
| | | | | | 3319 | 3322 | 10 |

It is here that problems most likely arise, for the numerical reliability of an algorithm to solve matrix equations normally decreases as the rank of the matrix increases.

7.2 Other mismatched parameters

We now assess the system sensitivity to small mismatches in resonators' masses, locations and frequencies.

7.2.1 Resonator mass mismatches

If the *masses* are slightly non-equal then one can write

$$M_a = \eta \mathcal{M} (1 + \mu_a \eta^{1/2}) , \quad a = 1, \dots, J \quad (60)$$

where η can be defined e.g. as the ratio of the *average* resonator mass to the sphere's mass. It is immediately obvious from equation (60) that mass non-uniformities of the resonators only affect the main equations in *second order*, since resonator mass non-uniformities result, as we see, in corrections of order $\eta^{1/2}$ to $\eta^{1/2}$ itself, which is the very parameter of the perturbative expansions. The system is thus clearly *robust* to mismatches in the resonator masses of the type (60).

7.2.2 Errors in resonator locations

The same happens if the *locations* of the resonators have tolerances relative to a *pre-selected* distribution. For let \mathbf{n}_a be a set of resonator locations, for example the *TIGA* or the *PHC* positions, and let \mathbf{n}'_a be the real ones, close to the former:

$$\mathbf{n}'_a = \mathbf{n}_a + \mathbf{v}_a \eta^{1/2} , \quad a = 1, \dots, J \quad (61)$$

The values \mathbf{n}_a determine the eigenvalues ζ_a in equation (27), and they also appear as arguments to the spherical harmonics in the system response functions of sections 4–6. It follows from (61) by continuity arguments that

$$Y_{lm}(\mathbf{n}'_a) = Y_{lm}(\mathbf{n}_a) + O(\eta^{1/2}) \quad (62.a)$$

$$\zeta'_a = \zeta_a + O(\eta^{1/2}) \quad (62.b)$$

Inspection of the equations of sections 4–6 shows that both ζ_a and $Y_{lm}(\mathbf{n}_a)$ *always* appear within lowest order terms, and hence that corrections to them of the type (62) will affect those terms in *second order* again. We thus conclude that the system is also *robust* to small misalignments of the resonators relative to pre-established positions.

7.2.3 Resonator frequency mistunings

The resonator *frequencies* may also differ amongst them, so let

$$\Omega_a = \Omega (1 + \rho_a \eta^{1/2}) , \quad a = 1, \dots, J \quad (63)$$

To assess the consequences of this, however, we must go back to equation (86) and see what the coefficients in its series solutions of the type (89.a) are. The procedure is very similar to that of section 7.1, and will not be repeated here; the lowest order coefficient $\chi_{\frac{1}{2}}$ is seen to satisfy the algebraic equation

$$\det \left[\delta_{ab} - \frac{1}{\chi_{\frac{1}{2}}} \sum_{c=0}^J \frac{\chi_{ac}^{(n_0 l_0)} \delta_{cb}}{\chi_{\frac{1}{2}} - \rho_c} \right] = 0 \quad (64)$$

which reduces to (90) when all the ρ 's vanish, as expected. This appears to potentially have significant effects on our results to lowest order in $\eta^{1/2}$, but a more careful consideration of the facts shows that it is probably unrealistic to think of such large tolerances in resonator manufacturing as implied by equation (63) in the first place. In the *TIGA* experiment, for example [29], an error of order $\eta^{1/2}$ would amount to around 50 Hz of mistuning between resonators, an absurd figure by all means. In a full scale sphere (~ 40 tons, ~ 3 metres in diameter, ~ 800 Hz fundamental quadrupole frequency, $\eta \sim 10^{-5}$) the same error would amount to between 5 Hz and 10 Hz in resonator mistunings for the lowest frequency. This is probably excessive for a capacitive transducer, but may be realistic for an inductive one. With this exception, it is thus more appropriate to consider that resonator mistunings are at least of order η . If this is the case, though, we see once more that the system is quite insensitive to such mistunings.

Summing up the results of this section, one can say that the resonator system dynamics is quite *robust* to small (of order $\eta^{1/2}$) changes in its various parameters. The important exception is of course the effect of suspension drilling, which do result in significant changes relative to the ideally perfect device, but which can be relatively easily calculated. The theoretical picture is fully supported by experiment, as *robustness* in the parameters here considered has been reported in the real device [33].

8 Conclusions

A spherical GW antenna is a natural multi-mode device with very rich potential capabilities to detect GWs on earth. But such detector is not just a bare sphere, it requires a set of *motion sensors* to be practically useful. It appears that transducers of the *resonant* type are the best suited ones for an efficient performance of the detector. Resonators however significantly interact with the sphere, and they affect in particular its frequency spectrum and vibration modes in a specific fashion, which must be properly understood before reliable conclusions can be drawn from the system readout.

The main objective of this paper has been the construction and development of an elaborate theoretical model to describe the joint dynamics of a solid elastic sphere and a set of *radial motion* resonators attached to its surface at arbitrary locations, with the purpose to make predictions of the system characteristics and response, in principle with arbitrary mathematical precision.

The solutions to the equations of motion have been shown to be expressible as an ascending series in powers of the small “coupling constant” η , the ratio of the average resonator mass to the mass of the larger sphere. The *lowest order* approximation corresponds to terms of order $\eta^{1/2}$ and, to this order, previous results [33, 39, 28] are recovered. This, I hope, should contribute to clarify the nature of the approximations inherent in earlier approaches, and to better understand the physical reason for their remarkable accuracy [33].

In addition, the methods of this paper have permitted us to discover that there can be in fact transducer layouts alternative to the highly symmetric *TIGA*, and having potentially interesting practical properties. An example is the *PHC* distribution, which is based on a pentagonally symmetric set of 5 rather than 6 resonators per quadrupole mode sensed. This transducer distribution has the property that *mode channels* can be constructed from the resonators’ readouts, much in the same way as in the *TIGA* [31]. In the *PHC* however a new and distinctive characteristic is present: different *wave amplitudes* selectively couple to different *detector modes* having different frequencies, so that the antenna’s mode channels come at different rather than equal frequencies. The *PHC* philosophy can be extended to make a *multi-frequency* system by using resonators tuned to the first two quadrupole harmonics of the sphere *and* to the first monopole, an altogether 11 transducer set.

The assessment of *symmetry failure* effects, as well as other parameter departures from ideality, has also been subjected to analysis. The general scheme is again seen to be very well suited for the purpose, as the theory transparently shows that the system is *robust* against relative disturbances of order η or smaller in any system parameters, also providing a systematic procedure to assess larger tolerances —up to order $\eta^{1/2}$. The system is shown to still be robust to tolerances of this order in some of its parameters, whilst it is not to others. Included in the latter group is the effect of spherical

symmetry breaking due to system suspension in the laboratory, which causes *degeneracy lifting* of the sphere's eigenfrequencies, which split up into multiplets. A strong point is that, by use of mostly analytic algorithms, it has been possible to accurately reproduce the reportedly measured frequencies of the *LSU* prototype antenna [29] with the predicted precision of four decimal places. The also reported robustness of the system to resonator mislocations [33] is too in satisfactory agreement with the theoretical predictions.

The perturbative approach here adopted is naturally open to refined analysis of the system response in higher orders in η . For example, one can systematically address the weaker coupling of non-quadrupole modes, etc. It appears however that such refinements will be largely masked by *noise* in a real system, as shown by Merkowitz and Johnson [34], and this must therefore be considered first. So the next step is to include noise in the model and see its effect. Stevenson [39] has already made some progress in this direction, and partly assessed the characteristics of *TIGA* and *PHC*, but more needs to be done since not too high signal-to-noise ratios should realistically be considered in an actual GW detector. In particular, *mode channels* are at the basis of noise correlations and dependencies, as well as the errors in GW parameter estimation [35]. I do expect the analytic tools developed in this article to provide a powerful framework to address the fundamental problems of *noise* in a spherical GW antenna which, to my knowledge, have not yet received the detailed attention they require.

Acknowledgments

I am greatly indebted with Stephen Merkowitz both for his kind supply of the *TIGA* prototype data, and for continued encouragement and illuminating discussions. I am also indebted with Curt Cutler for addressing my attention to an initial error in the general equations of section 2, and with Eugenio Coccia for many discussions. M.A. Serrano gave me valuable help in some of the calculations of Appendix A.2 below, and this is gratefully acknowledged, too. I have received financial support from the Spanish Ministry of Education through contract number PB96-0384, and from Institut d'Estudis Catalans.

Appendices

A.1 Green functions for the multiple resonator system

The density of forces in the rhs of equation (2.a) happens to be of the *separable* type

$$\mathbf{f}(\mathbf{x}, t) = \sum_{\alpha} \mathbf{f}^{(\alpha)}(\mathbf{x}) g^{(\alpha)}(t) \quad (65)$$

where α is a suitable label. It is recalled from reference [24] that, in such circumstances, a formal solution can be written down for equation (2.a) in terms of a *Green function integral*, whereby the following orthogonal series expansion obtains:

$$\mathbf{u}(\mathbf{x}, t) = \sum_{\alpha} \sum_N \omega_N^{-1} f_N^{(\alpha)} \mathbf{u}_N(\mathbf{x}) g_N^{(\alpha)}(t) \quad (66)$$

where

$$f_N^{(\alpha)} \equiv \frac{1}{\mathcal{M}} \int_{\text{Sphere}} \mathbf{u}_N^*(\mathbf{x}) \cdot \mathbf{f}^{(\alpha)}(\mathbf{x}) d^3x \quad (67.a)$$

$$g_N^{(\alpha)}(t) \equiv \int_0^t g^{(\alpha)}(t') \sin \omega_N(t - t') dt' \quad (67.b)$$

Here, ω_N and $\mathbf{u}_N(\mathbf{x})$ are the eigenfrequencies and associated normalised wave-functions of the free sphere. Also, N is an abbreviation for a multiple index $\{nlm\}$. The generic index α is a label for the

different pieces of interaction happening in the system. I quote the result of the calculations of the terms needed in this paper:

$$f_{\text{resonators},N}^{(a)} = \frac{M_a}{\mathcal{M}} \Omega_a^2 [\mathbf{n}_a \cdot \mathbf{u}_N^*(\mathbf{x}_a)] , \quad a = 1, \dots, J \quad (68.a)$$

$$f_{\text{GW},N}^{(l'm')} = a_{nl} \delta_{ll'} \delta_{mm'} , \quad N \equiv \{nlm\} , \quad l' = 0, 2 , \quad m' = -l', \dots, l' \quad (68.b)$$

$$f_{\text{stroke},N} = \mathcal{M}^{-1} \mathbf{f}_0 \cdot \mathbf{u}_N^*(\mathbf{x}_0) \quad (68.c)$$

where the coefficients a_{nl} in (68.b) are overlapping integrals of the type (67.a), and

$$g_{\text{resonators},N}^{(a)}(t) = \int_0^t [z_a(t') - u_a(t)] \sin \omega_N(t - t') dt' , \quad a = 1, \dots, J \quad (69.a)$$

$$g_{\text{GW},N}^{(lm)}(t) = \int_0^t g^{(lm)}(t') \sin \omega_N(t - t') dt' \quad (69.b)$$

$$g_{\text{stroke},N}(t) = \sin \omega_N t \quad (69.c)$$

If this is replaced into (2.a) one readily finds

$$\mathbf{u}(\mathbf{x}, t) = \sum_N \omega_N^{-1} \mathbf{u}_N(\mathbf{x}) \left\{ \sum_{b=1}^J \frac{M_b}{\mathcal{M}} \Omega_b^2 [\mathbf{n}_b \cdot \mathbf{u}_N^*(\mathbf{x}_b)] g_{\text{resonators},N}^{(b)}(t) + \sum_{\alpha} f_{\text{external},N}^{(\alpha)} g_{\text{external},N}^{(\alpha)}(t) \right\} \quad (70)$$

where the label “external” explicitly refers to agents acting upon the system from outside. Two kinds of such external actions are considered in this article: those due to GWs and those due to a calibration hammer stroke signal. Specifying $\mathbf{x} = \mathbf{x}_a$ in the lhs of (70) and multiply on either side by \mathbf{n}_a , the following is readily found:

$$u_a(t) = u_a^{\text{external}}(t) + \sum_{b=1}^J \eta_b \int_0^t K_{ab}(t - t') [z_b(t') - u_b(t')] dt' \quad (71.a)$$

$$\ddot{z}_a(t) = \xi_a^{\text{external}}(t) - \Omega_a^2 [z_a(t) - u_a(t)] , \quad a = 1, \dots, J \quad (71.b)$$

where $\eta_b \equiv M_b/\mathcal{M}$, $u_a^{\text{external}}(t) \equiv \mathbf{n}_a \cdot \mathbf{u}^{\text{external}}(\mathbf{x}_a, t)$,

$$\mathbf{u}^{\text{external}}(\mathbf{x}, t) = \sum_{\alpha} \sum_N \omega_N^{-1} f_{\text{external},N}^{(\alpha)} \mathbf{u}_N(\mathbf{x}) g_{\text{external},N}^{(\alpha)}(t) \quad (72)$$

and

$$K_{ab}(t) \equiv \Omega_b^2 \sum_N \omega_N^{-1} [\mathbf{n}_b \cdot \mathbf{u}_N^*(\mathbf{x}_b)] [\mathbf{n}_a \cdot \mathbf{u}_N(\mathbf{x}_a)] \sin \omega_N t \quad (73)$$

The following bare sphere responses to GWs and hammer strokes (equations (1) and (9), respectively) can be calculated by direct substitution. The results as best presented as Laplace transform domain functions:

$$\hat{u}_a^{\text{GW}}(s) = \sum_{\substack{l=0 \text{ and } 2 \\ m=-l, \dots, l}} \left(\sum_{n=1}^{\infty} \frac{a_{nl} A_{nl}(R)}{s^2 + \omega_{nl}^2} \right) Y_{lm}(\mathbf{n}_a) \hat{g}^{(lm)}(s) , \quad a = 1, \dots, J \quad (74.a)$$

$$\hat{u}_a^{\text{stroke}}(s) = - \sum_{nl} \frac{f_0}{s^2 + \omega_{nl}^2} |A_{nl}(R)|^2 P_l(\mathbf{n}_a \cdot \mathbf{n}_0) , \quad a = 1, \dots, J \quad (74.b)$$

where Y_{lm} are spherical harmonics and P_l Legendre polynomials [15]. The calculation of the Laplace transform of the kernel matrix (73) is likewise immediate:

$$\hat{K}_{ab}(s) = \sum_N \frac{\Omega_b^2}{s^2 + \omega_N^2} [\mathbf{n}_b \cdot \mathbf{u}_N^*(\mathbf{x}_b)] [\mathbf{n}_a \cdot \mathbf{u}_N(\mathbf{x}_a)] \quad (75)$$

Given that (see [24] for full details)

$$\mathbf{u}_{nlm}(\mathbf{x}) = A_{nl}(r) Y_{lm}(\theta, \varphi) \mathbf{n} - B_{nl}(r) i\mathbf{n} \times \mathbf{L} Y_{lm}(\theta, \varphi) \quad (76)$$

and that the spheroidal frequencies ω_{nl} are $2l+1$ -fold degenerate, (75) can be easily summed over the degeneracy index m , to obtain

$$\hat{K}_{ab}(s) = \sum_{nl} \frac{\Omega_b^2}{s^2 + \omega_{nl}^2} |A_{nl}(R)|^2 \left[\sum_{m=-l}^l Y_{lm}^*(\mathbf{n}_b) Y_{lm}(\mathbf{n}_a) \right] \quad (77)$$

or, equivalently,

$$\hat{K}_{ab}(s) = \sum_{nl} \frac{\Omega_b^2}{s^2 + \omega_{nl}^2} |A_{nl}(R)|^2 \frac{2l+1}{4\pi} P_l(\mathbf{n}_a \cdot \mathbf{n}_b) \quad (78)$$

where use has been made of the summation formula for the spherical harmonics [15]

$$\sum_{m=-l}^l Y_{lm}^*(\mathbf{n}_b) Y_{lm}(\mathbf{n}_a) = \frac{2l+1}{4\pi} P_l(\mathbf{n}_a \cdot \mathbf{n}_b) \quad (79)$$

and where P_l is a Legendre polynomial:

$$P_l(z) = \frac{1}{2^l l!} \frac{d^l}{dz^l} (z^2 - 1)^l \quad (80)$$

A.2 System response algebra

From equation (23), i.e.,

$$\sum_{b=1}^J \left[\delta_{ab} + \eta \sum_{nl} \frac{\Omega^2 s^2}{(s^2 + \Omega^2)(s^2 + \omega_{nl}^2)} \chi_{ab}^{(nl)} \right] \hat{q}_b(s) = -\frac{s^2}{s^2 + \Omega^2} \hat{u}_a^{\text{GW}}(s) + \frac{\hat{\xi}_a^{\text{GW}}(s)}{s^2 + \Omega^2}, \quad (\Omega = \omega_{n_0 l_0}) \quad (81)$$

we must first isolate $\hat{q}_b(s)$, then find inverse Laplace transforms to revert to time domain quantities. Substituting the values of $\hat{u}_a^{\text{GW}}(s)$ and $\hat{\xi}_a^{\text{GW}}(s)$ from (74.a) and (24) into (81) we find

$$\hat{q}_a(s) = \sum_{\substack{l=0 \text{ and } 2 \\ m=-l, \dots, l}} \hat{\Phi}_a^{(lm)}(s) \hat{g}^{(lm)}(s), \quad a = 1, \dots, J \quad (82)$$

where

$$\hat{\Phi}_a^{(lm)}(s) = -\frac{s^2}{s^2 + \Omega^2} \left(-\frac{R}{s^2} + \sum_{n=1}^{\infty} \frac{a_{nl} A_{nl}(R)}{s^2 + \omega_{nl}^2} \right) \sum_{b=1}^J \left[\delta_{ab} + \eta \sum_{nl} \frac{\Omega^2 s^2}{(s^2 + \Omega^2)(s^2 + \omega_{nl}^2)^2} \chi_{ab}^{(nl)} \right]^{-1} Y_{lm}(\mathbf{n}_b) \quad (83)$$

Now, using the convolution theorem of Laplace transforms, we see that the time domain version of equation (82) is

$$q_a(t) = \sum_{lm} \int_0^t \Phi_a^{(lm)}(t-t') g^{(lm)}(t') dt' , \quad a = 1, \dots, J \quad (84)$$

where $\Phi_a^{(lm)}(t)$ is the *inverse Laplace transform* of (83). The inverse Laplace transform of $\hat{\Phi}_a^{(lm)}(s)$ can be expediently calculated by the *residue theorem* through the formula

$$\Phi_a^{(lm)}(t) = 2\pi i \sum \left\{ \text{residues of } \left[\hat{\Phi}_a^{(lm)}(s) e^{st} \right] \text{ at its poles in complex } s - \text{plane} \right\} \quad (85)$$

Clearly thus, the *poles* of $\hat{\Phi}_a^{(lm)}(s)$ must be determined in the first place. It is immediately clear from equation (83) that there are no poles at either $s=0$, or $s=\pm i\Omega$, or $s=\pm i\omega_{nl}$, for there are exactly compensated infinities at these locations. The only possible poles lie at those values of s for which the matrix in square brackets in (83) is not invertible, and these of course correspond to the zeroes of its determinant, i.e.,

$$\Delta(s) \equiv \det \left[\delta_{ab} + \eta \frac{s^2}{s^2 + \Omega^2} \hat{K}_{ab}(s) \right] = 0 , \quad \text{poles} \quad (86)$$

There are infinitely many roots for equation (86), but *analytic* expressions cannot be found for them. *Perturbative* approximations in terms of the small parameter η will thus be applied instead. It is assumed that

$$\Omega = \omega_{n_0 l_0} \quad (87)$$

for a *fixed* multipole harmonic $\{n_0 l_0\}$. Equation (86) can then be recast in the more convenient form

$$\Delta(s) \equiv \det \left[\delta_{ab} + \eta \frac{\Omega^2 s^2}{(s^2 + \Omega^2)^2} \chi_{ab}^{(n_0 l_0)} + \eta \sum_{nl \neq n_0 l_0} \frac{\Omega^2 s^2}{(s^2 + \Omega^2)(s^2 + \omega_{nl}^2)} \chi_{ab}^{(nl)} \right] = 0 \quad (88)$$

Since η is a small parameter, the *denominators* of the fractions in the different terms in square brackets in (88) must be *quantities of order η* at the root locations for the determinant to vanish at them. A distinction however arises depending on whether s^2 is close to $-\Omega^2$ or to the other $-\omega_{nl}^2$. There are accordingly two categories of roots, more precisely:

$$s_0^2 = -\Omega^2 \left(1 + \chi_{\frac{1}{2}} \eta^{1/2} + \chi_1 \eta + \dots \right) \quad (\Omega = \omega_{n_0 l_0}) \quad (89.a)$$

$$s_{nl}^2 = -\omega_{nl}^2 \left(1 + b_1^{(nl)} \eta + b_2^{(nl)} \eta^2 + \dots \right) \quad (nl \neq n_0 l_0) \quad (89.b)$$

The coefficients $\chi_{\frac{1}{2}}, \chi_1, \dots$ and $b_1^{(nl)}, b_2^{(nl)}, \dots$ can be calculated recursively, starting from the first, by substitution of the corresponding series expansions into equation (88). The lowest order terms are easily seen to be given by

$$\det \left[\delta_{ab} - \frac{1}{\chi_{\frac{1}{2}}^2} \chi_{ab}^{(n_0 l_0)} \right] = 0 \quad (90)$$

and

$$\det \left[\frac{\Omega^2 - \omega_{nl}^2}{\omega_{nl}^2} b_1^{(nl)} \delta_{ab} - \chi_{ab}^{(nl)} \right] = 0 \quad (91)$$

respectively. Both equations (90) and (91) are algebraic eigenvalue equations. As shown in appendix A.3, the matrix $\chi_{ab}^{(nl)}$ has at most $(2l+1)$ non-null positive eigenvalues —all the rest up to J are identically zero.

As a final step we must evaluate (85). This is accomplished by standard textbook techniques (see e.g. [37]); the algebra is quite straightforward but rather lengthy, and I shall not delve into its details here, but quote only the most interesting results. It appears that the *dominant* contribution to $\Phi_a^{(lm)}(t)$ comes from the poles at the locations (89.a), whereas all other poles only contribute as higher order corrections; generically, $\Phi_a^{(lm)}(t)$ is seen to have the form

$$\Phi_a^{(lm)}(t) \propto \eta^{-1/2} \sum_{\zeta_c \neq 0} (\sin \omega_{c+} t - \sin \omega_{c-} t) \delta_{ll_0} + O(0) \quad (92)$$

where

$$\omega_{a\pm}^2 = \Omega^2 \left(1 \pm \sqrt{\frac{2l+1}{4\pi}} |A_{n_0 l_0}(R)| \zeta_a \eta^{1/2} \right) + O(\eta), \quad a = 1, \dots, J \quad (93)$$

In Laplace domain one has,

$$\hat{\Phi}_a^{(lm)}(s) \propto \eta^{-1/2} \sum_{\zeta_c \neq 0} \left[(s^2 + \omega_{c+}^2)^{-1} - (s^2 + \omega_{c-}^2)^{-1} \right] \delta_{ll_0} \quad (94)$$

Detailed calculation of the residues [38] yield equation (26), which must be evaluated for each particular tuning and resonator distribution, as described in section 4.

A.3 Eigenvalue properties

This Appendix presents a few important properties of the matrix $P_l(\mathbf{n}_a \cdot \mathbf{n}_b)$ for arbitrary l and resonator locations \mathbf{n}_a ($a=1, \dots, J$) which are useful for detailed system resonance characterisation.

Recall the *summation formula* for spherical harmonics [15]:

$$\sum_{m=-l}^l Y_{lm}^*(\mathbf{n}_a) Y_{lm}(\mathbf{n}_b) = \frac{2l+1}{4\pi} P_l(\mathbf{n}_a \cdot \mathbf{n}_b), \quad a, b = 1, \dots, J \quad (95)$$

where P_l is a Legendre polynomial

$$P_l(z) = \frac{1}{2^l l!} \frac{d^l}{dz^l} (z^2 - 1)^l \quad (96)$$

To ease the notation I shall use the symbol \mathcal{P}_l to mean the entire $J \times J$ matrix $P_l(\mathbf{n}_a \cdot \mathbf{n}_b)$, and introduce Dirac *kets* $|m\rangle$ for the column J -vectors

$$|m\rangle \equiv \sqrt{\frac{4\pi}{2l+1}} \begin{pmatrix} Y_{lm}(\mathbf{n}_1) \\ \vdots \\ Y_{lm}(\mathbf{n}_J) \end{pmatrix}, \quad m = -l, \dots, l \quad (97)$$

These kets are *not* normalised; in terms of them equation (95) can be rewritten in the more compact form

$$\mathcal{P}_l = \sum_{m=-l}^l |m\rangle \langle m| \quad (98)$$

Equation (98) indicates that the *rank* of the matrix \mathcal{P}_l cannot exceed $(2l+1)$, as there are only $(2l+1)$ kets $|m\rangle$. So, if $J > (2l+1)$ then it has at least $(J - 2l - 1)$ identically null eigenvalues —there can be more if some of the \mathbf{n}_a 's are parallel, as this causes rows (or columns) of \mathcal{P}_l to be repeated.

We now prove that the non-null eigenvalues of \mathcal{P}_l are *positive*. Clearly, a regular eigenvector, $|\phi\rangle$, say, of \mathcal{P}_l will be a linear combination of the kets $|m\rangle$:

$$\mathcal{P}_l |\phi\rangle = \zeta^2 |\phi\rangle, \quad |\phi\rangle = \sum_{m=-l}^l \phi_m |m\rangle \quad (99)$$

where ζ^2 is the corresponding eigenvalue, having a positive value, as we now prove. If the second (99) is substituted into the first then it is immediately seen that

$$\sum_{m'=-l}^l \left(\zeta^2 \delta_{mm'} - \langle m|m' \rangle \right) \phi_{m'} = 0 \quad (100)$$

which admits non-trivial solutions if and only if

$$\det \left(\zeta^2 \delta_{mm'} - \langle m|m' \rangle \right) = 0 \quad (101)$$

In other words, ζ^2 are the eigenvalues of the $(2l+1) \times (2l+1)$ matrix $\langle m|m' \rangle$, which is positive definite because so is the “scalar product” $\langle \phi|\phi' \rangle$. All of them are therefore strictly positive.

Finally, since the *trace* is an invariant property of a matrix, and

$$\text{trace}(\mathcal{P}_l) \equiv \sum_{a=1}^J P_l(\mathbf{n}_a \cdot \mathbf{n}_a) = \sum_{a=1}^J 1 = J \quad (102)$$

we see that the eigenvalues ζ_a^2 add up to J :

$$\text{trace}(\mathcal{P}_l) = \sum_{a=1}^J \zeta_a^2 \equiv \sum_{\zeta_a \neq 0} \zeta_a^2 = J \quad (103)$$

References

- [1] Ashby N. and Dreitlein J., 1975, PRD, 12, 336
- [2] Astone P. et al., 1993, PRD, 47, 2
- [3] Astone P. et al., 1997b, “*SFERA*: Proposal for a spherical GW detector”, Roma
- [4] Bianchi M., Coccia E., Colacino C. N., Fafone V., Fucito F., 1996 CQG, 13, 2865
- [5] Bianchi M., Brunetti M., Coccia E., Fucito F., Lobo J. A., 1998, PRD, 57, 4525
- [6] Brans C. and Dicke R. H., 1961, Physical Review, 124, 925
- [7] Coccia E., Lobo J. A., Ortega J. A., 1995a, PRD, 52, 3735
- [8] Coccia E., Pizzella G., Ronga F., eds., 1995b, Proceedings of the First Edoardo Amaldi Conference, World Scientific, Singapore
- [9] Astone P. *et al*, *Phys. Rev.* **D47**, 2 (1993).
- [10] Coccia E. and Fafone V., 1996, Physics Letters A, 213, 16
- [11] Coccia E., 1997, in Francaviglia M., Longhi G., Lusanna L., and Sorace E., eds., Proceedings of the GR-14 Conference, World Scientific, Singapore
- [12] Coccia E., Fafone V., Frossati G., Lobo J. A. and Ortega J. A., 1998, PRD, 57, 2051
- [13] Dhurandhar S. V., Krolak A., Lobo J. A., 1989, MNRAS, 237, 333, and MNRAS, 238, 1407

- [14] Dhurandhar S. V. and Tinto M., 1989, MNRAS, 236, 621
- [15] Edmonds A. R., 1960, Angular Momentum in Quantum Mechanics, Princeton University Press
- [16] Forward F., 1971, Gen. Rel. and Grav., 2, 149
- [17] Hamilton W. O., Johnson W. W., Xu B. X., Solomonson N., Aguiar O. D., 1989, PRD, 40, 1741
- [18] Har'El Z., 1993, Geometriae Dedicata, 47, 57
- [19] Helstrom C. W., 1968, Statistical Theory of Signal Detection, Pergamon Press, Oxford
- [20] Holden A., 1977, Formes, espace et symétries, CEDIC, Paris
- [21] Johnson W. W. and Merkowitz S. M., 1993, PRL, 70, 2367
- [22] Krolak A., Lobo J. A., Meers B. J., 1991, PRD, 43, 2470
- [23] Landau L. D. and Lifshitz E.M., 1970, Theory of Elasticity, Pergamon Press, Oxford
- [24] Lobo J. A., PRD, 52, 591
- [25] Lobo J. A. and Serrano M. A., 1996, Europhysics Letters, 35, 253
- [26] Lobo J. A. and Serrano M. A., 1997, CQG, 14, 1495
- [27] Magalhães N. S., Johnson W.W., Frajuca C, Aguiar O., 1995, MNRAS, 274, 670
- [28] Magalhães N. S., Aguiar O. D., Johnson W. W., Frajuca C., 1997, GRG, 29, 1509
- [29] Merkowitz S. M., 1995, PhD Thesis, Louisiana State University
- [30] Merkowitz S. M., 1998, PRD, 58, 062002
- [31] Merkowitz S. M. and Johnson W. W., 1995, PRD, 51, 2546
- [32] Merkowitz S. M. and Johnson W. W., 1996, PRD, 53, 5377
- [33] Merkowitz S. M. and Johnson W. W., 1997, PRD, 56, 7513
- [34] Merkowitz S. M. and Johnson W. W., 1998, Europhysics Letters, 41, 355
- [35] Merkowitz S. M., Lobo J. A., Serrano M. A., 1999, CQG, 16, 3035
- [36] Merkowitz S. M., Coccia E., Fafone V., Raffone G., Schipilliti M., and Visco M., 1999, Rev Sci Instr, 70, 1553
- [37] Porter D. and Stirling D. S. G., 1990, Integral equations: a practical treatment from spectral theory to applications, Cambridge University Press
- [38] Serrano M. A., 1999, PhD Thesis, University of Barcelona
- [39] Stevenson T. R., 1997, PRD, 56, 564
- [40] Tricomi F. G., 1957, Integral equations, Interscience Publishers
- [41] Wagoner R. V. and Paik H. J., 1977, in Proceedings of the Pavia International Symposium, Accademia Nazionale dei Lincei, Roma

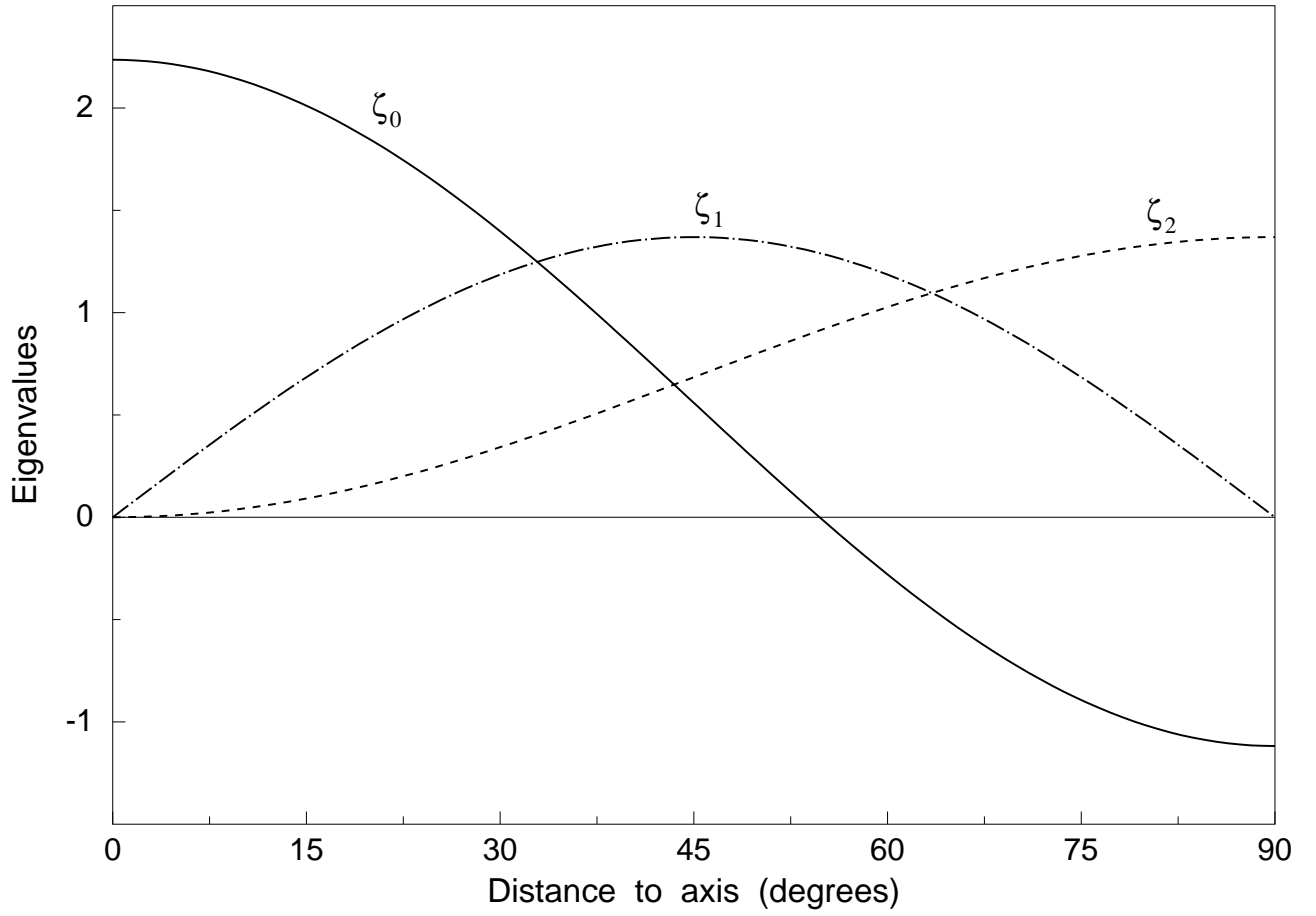


Figure 2: The three distinct eigenvalues ζ_m ($m=0,1,2$) as functions of the distance of the resonator parallel's co-latitude α relative to the axis of symmetry of the distribution, cf. equation (39.a).

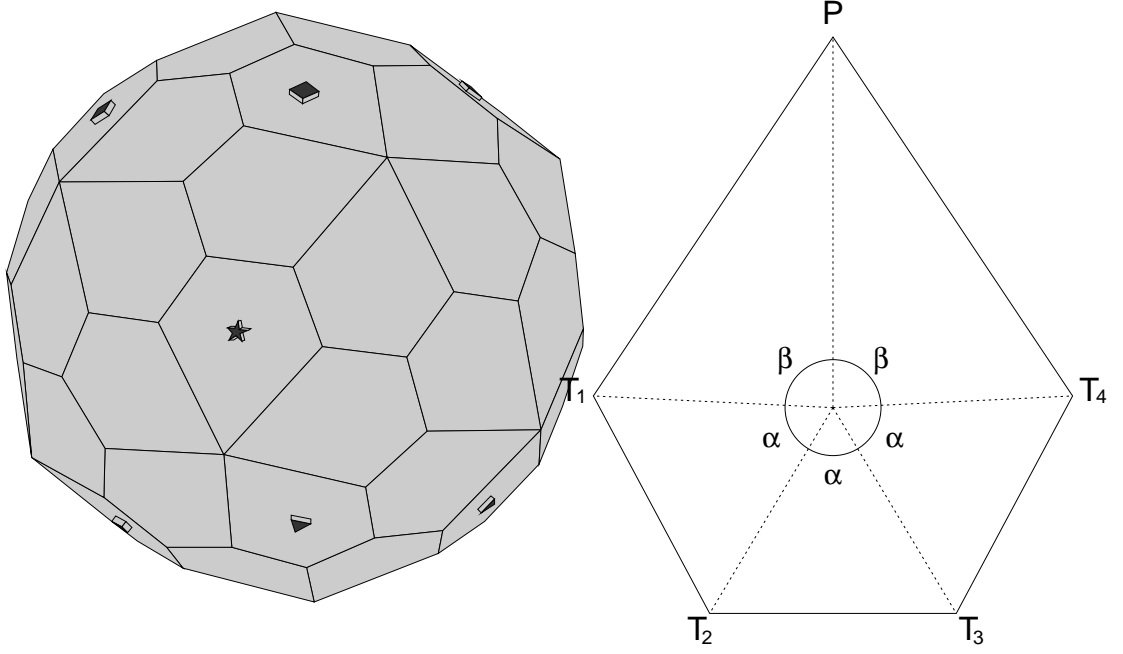


Figure 3: To the left, the *pentagonal hexacontahedron* shape. Certain faces are marked to indicate resonator positions in a specific proposal —see text— as follows: a *square* for resonators tuned to the first quadrupole frequency, a *triangle* for the second, and a *star* for the monopole. On the right we see the (pentagonal) face of the polyhedron. A few details about it: the confluence point of the dotted lines at the centre is the tangency point of the *inscribed* sphere to the *PHC*; the labeled angles have values $\alpha = 61.863^\circ$, $\beta = 87.205^\circ$; the angles at the *T*-vertices are all equal, and their value is 118.1366° , while the angle at *P* is 67.4536° ; the ratio of a long edge (e.g. PT_1) to a short one (e.g. T_1T_2) is 1.74985, and the radius of the inscribed sphere is *twice* the long edge of the pentagon, $R = 2PT_1$.

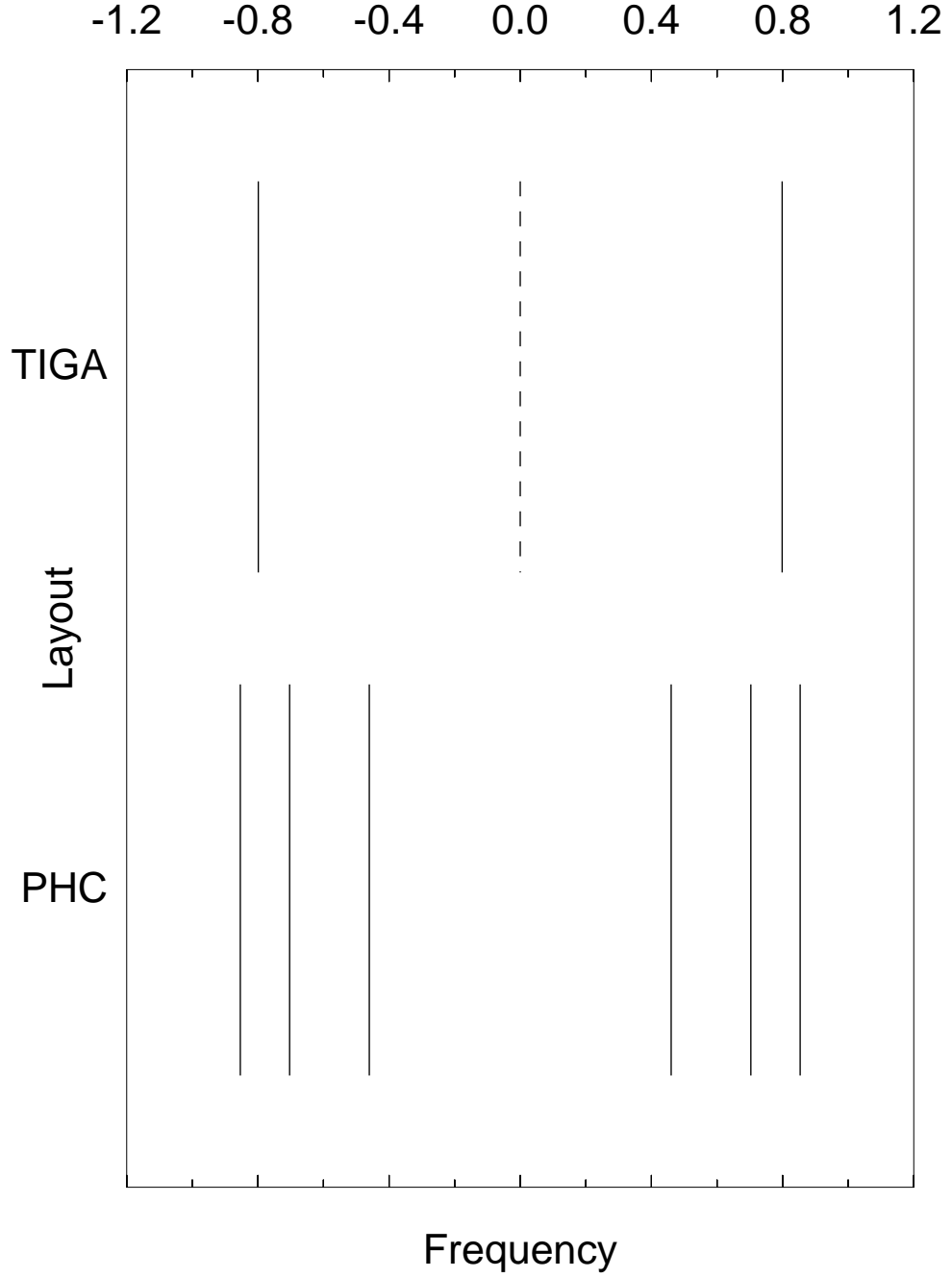


Figure 4: Compared line spectrum of a coupled *TIGA* and a *PHC* resonator layout in an ideally spherical system. The weakly coupled central frequency in the *TIGA* is drawn dashed. The frequency pair is 5-fold degenerate for this layout, while the two outer pairs of the *PHC* are doubly degenerate each, and the inner pair is non-degenerate. Units in abscissas are $\eta^{1/2}\Omega$, and the central value, labeled 0.0, corresponds to Ω .

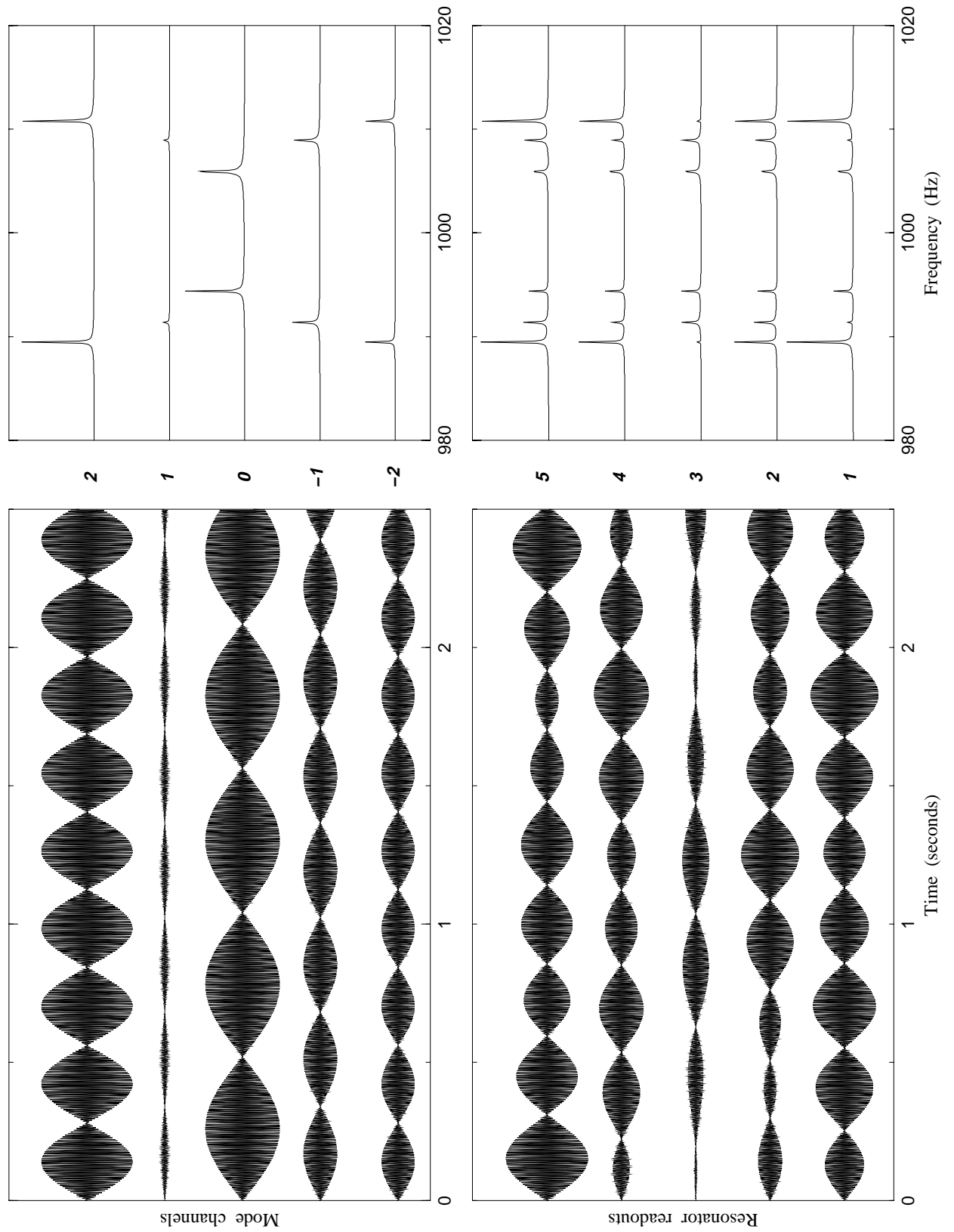


Figure 5: Simulated response of a *PHC* to a hammer stroke: the time series and their respective spectra, both for direct resonator readouts and mode channels. Note that while the former are *not* simple beats, the latter are.

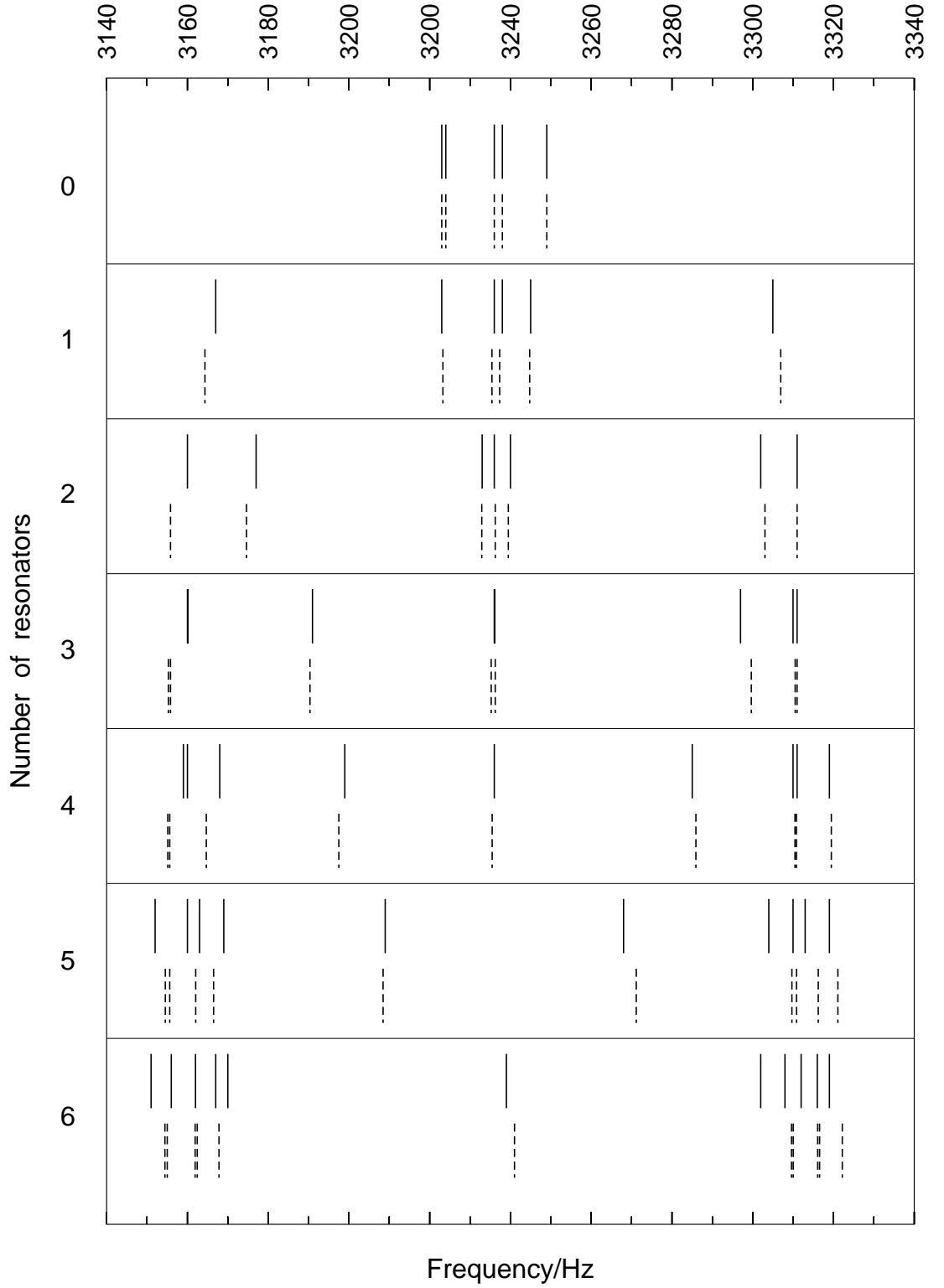


Figure 6: The frequency spectrum of the *TIGA* distribution as resonators are progressively added from none to 6. Continuous lines correspond to measured values, and dashed lines correspond to their $\eta^{1/2}$ theoretical estimates with equation (56).